Identification of water–rock interaction of surface thermal water in Songwe medium temperature geothermal area, Tanzania

Asnin, Sitti Nur; Nnko, Martha; Josephat, Sadock; Mahecha, Albano; Mshiu, Elisante; Bertotti, Giovanni; Brehme, Maren

ORIGINAL ARTICLE

Identification of water–rock interaction of surface thermal water in Songwe medium temperature geothermal area, Tanzania

Sitti Nur Asnin[1] · Martha Nnko[1,2] · Sadock Josephat[3] · Albano Mahecha[3] · Elisante Mshiu[2] · Giovanni Bertotti[1] · Maren Brehme[1,4]

Abstract

The Songwe geothermal prospect is situated in western Tanzania in the Rukwa Rift of the western branch of the East African Rift System. Thermal springs discharge along NW–SE oriented fracture zones in two separate areas: in the main Songwe graben (Iyola, Main springs, Rambo and Kaguri) and eastern Songwe graben (Ikumbi). Lithologies forming and filling the Songwe graben are metamorphic gneiss and shist as basement rocks, overlain by the Karoo sandstones, and Red sandstones, both silt- and sandstones with a carbonatic matrix. In some areas of the graben, volcanic rocks intruded these formations forming basalt outflows. The discharge temperatures of springs are between 37 and 85 °C with Na-HCO$_3$ type fluids. Carbonate deposits surround most of the springs. Using previous geophysical, geological studies and historical fluid geochemical data and mineral data, the Songwe geothermal system interpretation was updated, including new reservoir fluid temperature, fluid flow pathway and water–rock interaction models. The classical geothermometers of K-Mg and Na-K-Ca $_{(Mg\ correction)}$ were used to predict the reservoir fluid temperature and show that fluid emerging in the Songwe area reaches temperatures between 125 and 148 °C. Reservoir fluid characteristics are reconstructed based on the geothermometer calculation and a PHREEQC model in which the deep fluid reacts with certain lithologies. Minerals precipitating at the surface and reservoir depth were used to calibrate the models. The models run at surface temperature were calibrated with minerals precipitating around the springs and suggest that Songwe thermal fluids interact with Red sandstone only, while Ikumbi spring water is the only spring that interacts with all lithologies (simplified referred to as: metamorphic rocks, Karoo and Red sandstone). The model run at reservoir temperature indicates that rising water is also in contact with Karoo sandstones and Ikumbi spring water composition is again influenced by the contact with all lithologies in the graben. Our conceptual model summarizes all data showing the meteoric origin of the fluids, the travel through the basement, rising along the Mbeya fault and the main reaction with sandstones through a lateral travel towards the hot springs. The proposed models reinforce the idea that carbonate dissolution from the sandstone layers is the most common water–rock interaction. Our model is supported by carbonate deposition observed in all springs, dominated by HCO$_3$ and Na.

Keywords Songwe · Geothermal · Geochemical modelling · Water–rock interaction · Fluid source · Tanzania

Introduction

Geochemical investigations in the initial stage of geothermal field development typically aim for characterizing subsurface conditions to define drilling targets (Truesdell and Jones 1974). The geochemical information are obtained from geothermal surface manifestations. They do not only support temperature estimations but also give general information on the geothermal system such as hydrogeochemical processes, upflow, and/or outflow zones (Brehme et al., 2021; Nicholson 1993; White 1965, Ellis and Wilson 1960). Techniques usually applied are geochemical sampling and

✉ Maren Brehme
  mbrehme@ethz.ch

1 Department of Geoscience and Engineering, TU Delft,
  CN Delft 2628, the Netherlands

2 Department of Geology, University of Dar Es Salaam,
  P. O. Box 35052, Dar es Salaam, Tanzania

3 Tanzania Geothermal Development Company, P.O
  Box 14801, Dar es Salaam, Tanzania

4 Department of Earth Sciences, Geothermal Energy
  and Geofluids Group, ETH Zurich, 8092 Zurich, Switzerland

characterization of spring and reservoir water as well as mixing models to identify fluid sources, 2-phase proportions or mixing during fluid rise to surface (Truesdell and Jones 1974). Isotope studies help to identify the fluid source while geothermometers are used to estimate the reservoir temperature (Ellis and Wilson 1960). Equilibrium calculations of fluids with minerals are used to predict scaling tendencies (Giggenbach 1988a, b). In this study, the geochemical equilibration is used to identify the fluid source by comparing known precipitations to modelled fluid-rock interaction. By modelling the reaction of reservoir water with the different types of geological layers and comparing the results to measured minerals precipitated in that layer, we gain understanding of fluid pathways and sources.

Geochemical investigations related to geothermal energy exploration have been conducted in the Songwe field, Tanzania, since the late 1950s (see next paragraph). Located in western Tanzania in the Rukwa Rift of the western branch of the East African Rift System (EARS) the Songwe geothermal area has a significant resource with medium to high temperature thermal springs with carbonate or travertine-rich deposits (Hochstein et al. 2000). The system is located 50 km north of the Mbeya volcanic province.

James (1959) reported the first chemical analysis of thermal springs in the Songwe river valley. Using chemical data of the "Kaguri thermal spring" and gas samples of "Main hot springs", the author suggests the gas-bearing springs are of volcanic origin. Nzaro (1970) also analyzed the thermal springs throughout the valley with a focus on their relation to the block-faulted region of the rift system. Later, a Swedish consultant group SWECO (1978) carried out a geochemical sampling survey of surface manifestations in Tanzania, including the Songwe area, and considered it one of the high-temperature geothermal fields in Tanzania. Makundi and Kifua (1985) provide a chemical data inventory of thermal springs in the Mbeya prospect area. Applying the Na-K-Ca geothermometer, these authors argue that the estimated deep fluid temperature is ranging from 170 °C near the Ivuna springs (80 km NW of Songwe) to 217 °C at Songwe. The other geothermometers of thermal springs (chalcedony, K/Mg, Na/K geothermometer) suggest intermediate to high temperatures (100–255 °C) in the Songwe reservoir although these springs are described as outflow zone (Hochstein et al. 2000; Mnjokava 2007). Springs in outflow zones normally show low temperatures in contrast to the upflow zone of a geothermal system.

These various datasets and the yet uncertain understanding of the geothermal system in Mbeya area led to the implementation of the GEOTHERM technical cooperation program of BGR (Federal Institute for Geoscience and Natural Resources, Germany) that consisted of a geological, geochemical, and geophysical survey between 2006 and 2009 (Delvaux et al. 2010; Kalberkamp et al. 2010; Kraml et al.

2010). Results show a structurally controlled fluid flow and a close association of thermal springs with active strike-slip and normal faulting (Delvaux et al. 2010). Magnetotelluric and Transient Electromagnetic surveys conducted by Kalberkamp et al. (2010) show a low magnetic anomaly in the Songwe area indicating strong alteration in rocks. Thus, the GEOTHERM studies came up with the main conclusion that Songwe thermal springs are an outflow zone of Lake Ngozi volcanic hydrothermal system. Conversely, other authors distinguish between Songwe geothermal system and Ngozi volcano based on the recent studies on geology, geochemistry, and geophysics by TGDC (Tanzania Geothermal Development Co. Ltd) and UNEP (United Nations Environment Programme) in 2016 (Alexander et al. 2016; Hinz et al. 2018). These authors also conclude that many springs are not associated with large apparent faults.

In addition, major ion analyses and mineral composition of travertines in the Songwe area have been studied to understand its origin showing a close association of the travertine deposits with Neogene-Quaternary volcanism (Pisarskii et al. 1998). Additionally, U/Th travertine data suggest a link between volcanic and geothermal activities (Delvaux et al. 2010). It supports the argument of Alexander et al. (2016) that Songwe Sr-rich travertines derive from volcanic rocks.

Even though a number of previous geoscientific studies have been carried out in the Songwe area, a detailed understanding of fluid flow pathways and related water–rock interaction has not been achieved yet. Taking advantage of the history of fluid geochemical data and geological mineral data of distinct lithologies, the purpose of this study is to update the interpretation of the Songwe geothermal system and add information on geothermal fluid pathways and sources. It comprises of (1) the reservoir temperature estimation and (2) interpretation of fluid flow pathways related to structural geology and (3) the modelling of water-rock interaction. We synthesize our results in a fluid flow model of the Songwe geothermal field.

Geology and structural geology

Regional geological setting

As part of the western branch of the EARS, Songwe geothermal resources are situated in the long valley of the Songwe basin. The Songwe basin is a sub-basin of the Rukwa Rift Basin, which is a half-graben flanked by uplifted Proterozoic metamorphic rocks of the late Ubendian shear belt (Kilembe and Rosendahl 1992). Metamorphic rocks in Songwe area are composed of amphibolite, gneiss, schist, and mylonite (EAGER 2018). The Proterozoic gneissic rocks consist of high-grade migmatitic metasediments (biotite-garnet gneisses) that are underlain by igneous

rocks (hornblende-pyroxene gneisses and quartz-rich garnet pyroxene gneisses), and high-grade metamorphic rocks intruded by granodiorite and diorites (Harkin and Harpum 1978; Macfarlane 1966). These Proterozoic basement rocks (Fig. 1) are unconformably overlain by the Permo-Triassic Karoo group, Triassic Red sandstone, and Quaternary Volcanics (Fig. 1). In the western study area, the Permian-Triassic Karoo group is exposed at surface. These rocks are comprised of a series of glacial to periglacial strata, lacustrine, and fluvial deposits with conglomerates, siltstones and sandstone, carbonatic minerals and coal deposits (Alexander et al. 2016; Dypvik et al. 1990; Delvaux 2001; Roberts et al. 2004, 2010; Semkiwa et al. 1998). EAGER (2018) suggests the Karoo layers in the Songwe basin are mainly comprised of sandstone and conglomerate with about 500 m thickness.

In the NW and the SE of the study area, the Red sandstone is widespread with 1300–1500 m thickness (EAGER 2018). The rocks consist of quartz, K-feldspar, muscovite and apatite (Alexander et al. 2016). The Red sandstones are loosely packed sediments, which are often overlain by massive travertine with 5–20 m thickness in the surrounding of

thermal springs and extend towards the western basin margin (EAGER 2018). Additionally, fractures and pores in the Red sandstones are filled with carbonatic minerals. The Quaternary Volcanics are only deposited in the SE (Ikumbi) area and composed of trachyte and basalts (Alexander et al. 2016).

Structural geology of the Songwe basin

The geological cross section of the Songwe basin shows the basic geological units e.g. metamorphics as basement, overlain by Karoo Sandstones, Red Sandstones and partly volcanics (Fig. 2). The Mbeya fault in the NE of the basin cuts these units and underlines the graben structure. Sandstones and Volcanics are only found within the graben system and dip towards NE. Previous fluid-flow models suggest an infiltration of rainwater at the NE and SW edges of the basin, which is then heated at depth and rises through the sandstones to surface.

Associated with a rifting system, the Songwe basin is situated in an active structural set-up. The set-up has been investigated in several studies by (Alexander et al. 2016;
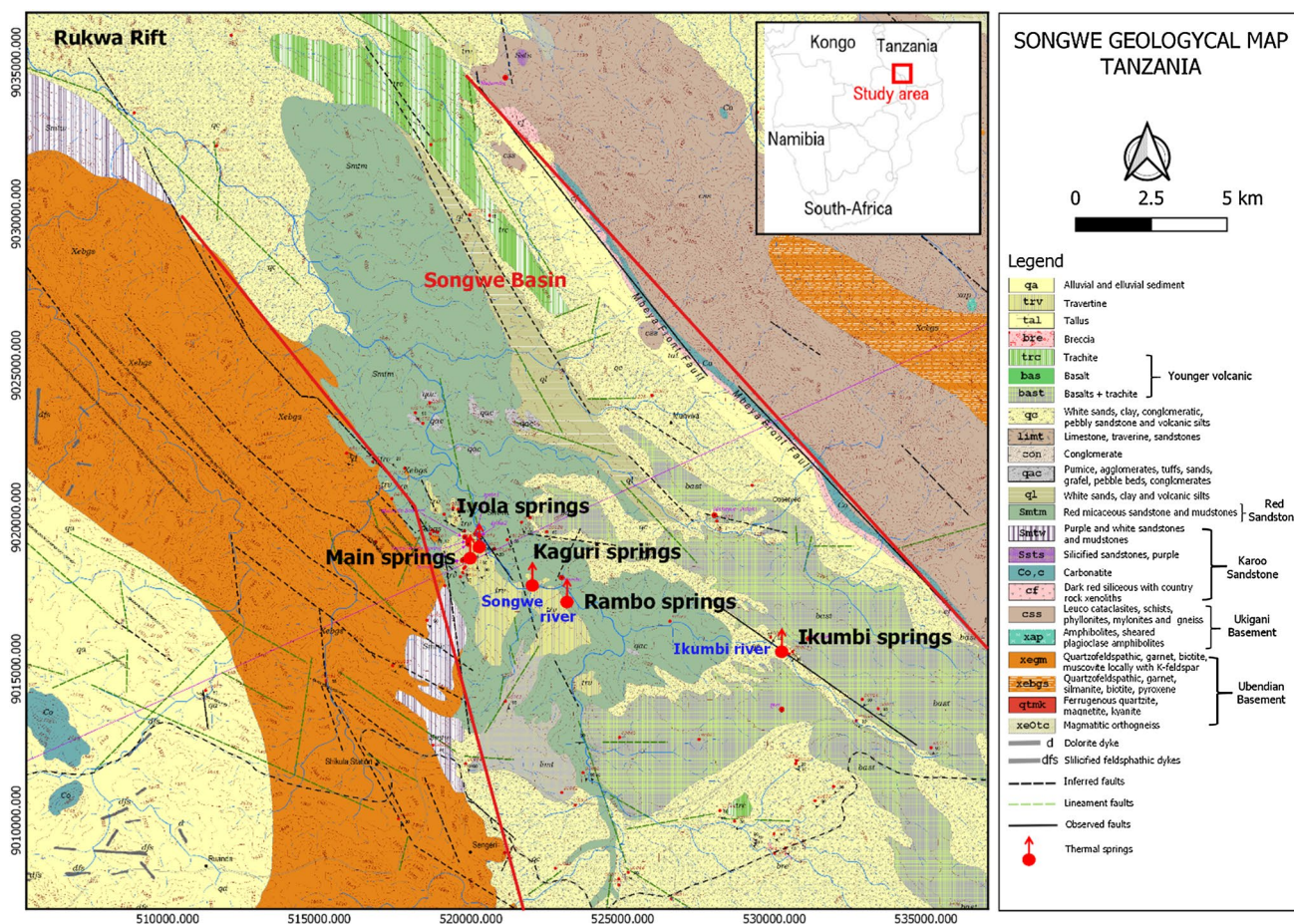

Fig. 1 Songwe geological map modified after Alexander et al. (2016), showing thermal spring locations
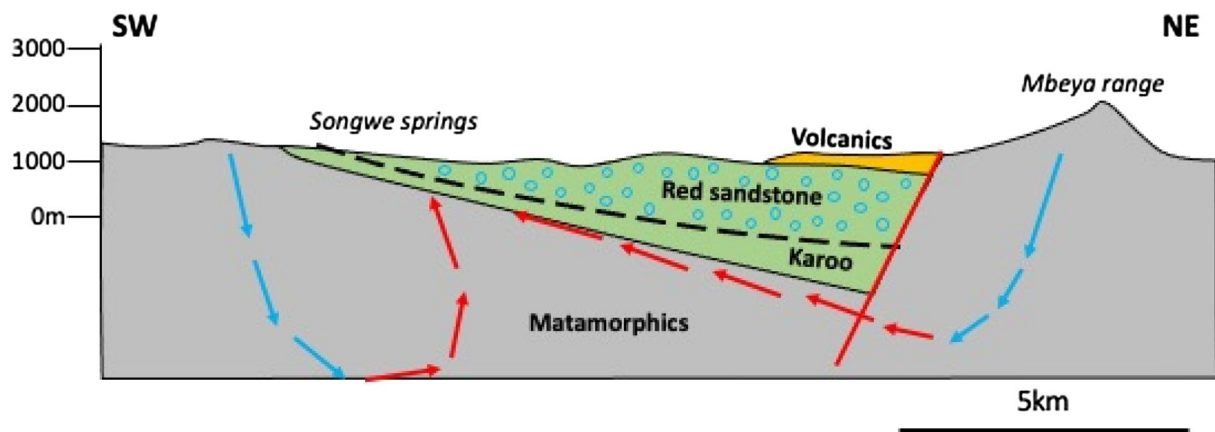
Fig. 2 Schematic section across the Songwe half-graben. The overall geometry of the basin is obtained combining surface data from Alexander et al., (2016). The deep part of the basin is inferred from EAGER (2018). The two reports provide a contrasting hypothesis for the position of the boundary between the Karoo and Red Sandstones (dashed line in our figure). The flow paths correspond to those predicted by Alexander et al. (2016)

Delvaux et al. 2010; EAGER 2018; Ebinger 1989; Hinz et al. 2018; Kilembe and Rosendahl 1992). All studies suggest a transtensional regime with strike-slip and normal faults. The main strike direction of the structures is corresponding to the basin in NW–SE direction.

Various studies differ slightly in their interpretation but show two major faults within the Songwe basin (Alexander et al. 2016; Delvaux et al. 2010; EAGER 2018). The Mbeya range fault is the NE boundary of the system and described as dextral strike slip or partly normal fault. Another major fault runs through the centre of the basin and is characterized as dextral strike-slip fault with a left step-over in the centre of the basin. This step-over zone is associated with fractures and accommodates most of the hot springs of the Songwe basin. Alexander et al. (2016) also suggested a fault at the SW boundary of the basin dipping as normal fault towards the basin. More recent studies by Hinz et al. (2018) additionally show fracture patterns and WNW striking, SW dipping normal faults within the basin. The detailed structural geology of the Songwe basin is subject of further studies by the authors of this paper and will be published in an additional format. Previous results confirm that the major dextral strike-slip fault in the basin centre provides locations of accompanying minor sinistral faults and a fracture pattern with normal displacement distributed over the basin.

Materials and methodology

Sampling and analysis

Water samples

A total of 17 geothermal springs from five spring groups were sampled during the first week of November 2019. The sampling locations are shown in Fig. 1. During the field survey, deposits around the thermal manifestations were described and physicochemical parameters were measured in-situ using portable instruments, including water temperature (T), acidity (pH), and specific electrical conductivity (EC). The sampling technique is applied according to hydrogeological procedures used by Brehme et al. (2010 and 2018). Water samples for chemical analysis were filtrated in-situ through 0.45 μm filter and stored in two 30 ml polyethylene bottles. Hydrochloric acid was added into one of the batches to lower the pH < 2 for cation analyses, while the other batch taken for anion analyses remained untreated.

The major ions were analyzed at the geochemical community laboratory of the Berlin Institute of Technology. Anion concentrations including Na^+, K^+, $Fe^{2+/3+}$, Ca^{2+}, and Mg^{2+} were determined by AAS (Analytik Jena, novAA 400) and ICP-OES Thermo Jarrel Ash with a detection limit of 0.02 ppm, 0.04 ppm, 0.0007 ppm, 0.007 ppm, and 0.003 ppm, respectively. Cations Cl^-, SO_4^{2-}, F^-, Br^-, NO_3^- and PO_4^{3-}, were determined using ion chromatography Dionex DX 120 with detection limit of 1.5 ppm, 2.5 ppm, 0.25 ppm, 0,75 ppm, 0.75 ppm, and 1 ppm, respectively. The HCO_3^- concentration was measured on-site using alkalinity titration.

The reliability of the major element analysis was evaluated based on ionic balance errors. An ionic balance error is calculated by comparing the molal concentration of anions and cations (meq). An ionic balance error ≤ 5% means that the accuracy of the chemical analysis is reliable (Nicholson 1993). Practically, almost all data from the major elements analysis in 2019 are within the preferred ion balance error (Table 1) except for Kaguri 1 (6.6%).

Table 1 Field parameter and chemical analysis of thermal manifestation in this study (2019) and other studies previously

Springs	Sampling date	Southing/Easting	Elevation (m)	T (°C)	Field pH	EC (µS/cm)	Na^+ (mg/L)	K^+	Ca^{2+}	Mg^{2+}	SiO_2	$Fe^{2+/3+}$	Li^+	B^{3+}	As^{3+}	Al^{3+}	HCO_3^-	SO_4^{2-}	Cl^-	Ionic Balance
Rambo old	11/5/2019	523,088/9017787	1125	82.7	6.5	2650	867.7	81.1	19	7.91	–	0.0031	0.79	0.63	–	–	1831	176.84	222.58	1.9
Rambo middle	11/5/2019	523,095/9017773	1124	70.2	6.7	2470	865.6	78.5	16	7.65	–	0.0011	0.78	0.62	–	–	1959	177.33	223.82	1.9
Rambo new	11/5/2019	523,100/9017753	1124	82.9	4.8	2910	851.1	84.6	24	8.08	–	0.0049	0.77	0.62	–	–	1885	176.67	222.49	1.2
Kaguri 1	11/7/2019	521,978/9018143	1078	70.9	8.6	2790	867.8	85.1	17	8.46	–	0.0068	0.74	0.60	–	–	1623	176.27	218.62	6.6
Kaguri 2	11/7/2019	522,049/9018065	1080	48	8	2570	979.9	88.4	41	9.76	–	0.0113	0.73	0.61	–	–	2248	178.24	216.12	1.3
Kaguri 3	11/7/2019	522,007/9018206	1079	62.9	5.8	2760	874.4	68.7	18	8.33	–	0.0129	0.70	0.59	–	–	2032	175.45	216.39	1.8
Main spring 1	11/5/2019	520,034/9019037	1119	75	6.6	2640	840.4	88.5	47	13.9	–	0.0851	0.73	0.58	–	–	2123	174.52	195.14	1.7
Main spring 2	11/5/2019	520,036/9019046	1127	75.5	6.2	2730	823.9	87.5	37	14.9	–	0.0046	0.72	0.57	–	–	1934	171.9	193.75	0.7
Main spring 3	11/5/2019	520,046/9019135	1119	73.2	6.4	2870	862.1	90	37	16.3	–	0.0025	0.70	0.56	–	–	1922	171.56	192.59	3.1
Main spring 4	11/5/2019	520,032/9019171	1127	68.7	6.5	2240	803.1	73.1	38	18	–	0.0019	0.69	0.55	–	–	1916	169.94	188.25	0.02
Iyola 1	11/5/2019	520,249/9019413	1057	74.4	6.8	3600	818	107	61	23.7	–	0.0073	0.61	0.49	–	–	2166	168.83	175.78	0.6
Iyola 2	11/5/2019	520,310/9019418	1064	62	6.4	2920	824	105	44	21.2	–	0.013	0.60	0.49	–	–	2026	168.01	178.63	0.8
Ikumbi 1	11/6/2019	529,873/9016237	1211	43.9	7.1	420	116.1	46	12	4.78	–	0.0026	0.02	0.011	–	–	458	5.44	8.89	4.1
Ikumbi 2	11/6/2019	530,101/9015910	1217	42	6.4	470	115.2	44.1	16	5.97	–	0.0005	0.02	0.004	–	–	439	5.04	7.94	0.8
Ikumbi 3	11/6/2019	530,212/9015896	1214	38.2	8.2	450	119.4	45.6	15	5.85	–	0.0005	0.02	0.004	–	–	430	5.09	8.08	1.4
Ikumbi 4	11/6/2019	530,291/9015840	1204	41.3	7.9	440	120.9	46.1	14	5.24	–	0.0018	0.02	0.023	–	–	439	5.48	9.12	0.01
Ikumbi 5	11/6/2019	530,319/9015818	1210	37.1	7.5	410	116.8	45.9	15	5.44	–	0.0165	0.02	0.028	–	–	458	5.72	8.13	2.6
Rambo 2016[a]	1/23/2016		1129	80.2	7.6	3760	774	103	29.5	3.2	63	–	–	0.19	–	–	1976	430	217	11
Main spring 2016[a]	1/19/2016	520,042/9019043	1129	74.7	7.2	3830	745	113	20.9	15.6	72	–	–	0.17	–	–	2247	166	199	9.8
Rambo 1–2008[c]	6/7/2006	523,058/9017886	1127	72	nd	3700	806	83.4	10.4	7.9	68.1	0.011	0.758	0.725	0.143	0.007	–	139	181	65.7
Rambo 2–2008[c]	6/7/2006	522,966/9018008	1087	80.2	nd	3800	818	82	17.1	8	70.3	0.177	0.762	0.727	0.149	0.371	–	143	184	65.8
Rambo 3–2008[c]	11/1/2006	522,966/9018008	1088	65	7.1	3600	828	91.4	16.5	9.2	68.5	0.007	0.761	0.667	0.099	0.04	2350	146	196	7.9
Rambo 4–2008[c]	6/7/2006	523,025/9018021	1087	74.1	nd	3700	821	83.5	15.9	8.5	68.9	0.03	0.751	0.717	0.141	0.056	–	138	180	66.6
Main spring 1–2008[c]	11/3/2006	520,022/9019159	1140	74	nd	3700	802	102	21	16.2	74.2	0.024	0.725	0.621	0.113	0.004	–	146	175	66.9
Main spring 2–2008[c]	6/27/2007	520,112/9018786	1156	60.3	6.7	3830	775	95.4	30.3	15.6	71.8	0.125	0.696	0.614	0.145	0.023	3061	154	197	19.9
Ikumbi 1–2008[c]	7/1/2007	530,101/9015912	1236	42.4	6.7	650	100	46.9	15.5	5.8	124	0.003	0.0175	–	0.0015	0.003	683	0.98	8.2	26
Ikumbi 2–2008[c]	7/1/2007	529,870/9016233	1216	44.1	6.9	640	106	48.7	12.1	4.5	133	0.003	0.0206	0.0051	0.0018	0.007	583	1.72	9	18
Ikumbi 3–2008[c]	7/1/2007	530,359/9015768	1226	38.5	7	670	102	48.3	15.5	5.7	126	0.01	0.0171	–	0.0016	0.005	559	0.91	8.3	15
Ikumbi 4–2008[c]	7/1/2007	530,357/9015794	1227	44.1	6.8	670	102	48.7	13.5	4.9	125	0.001	0.0206	–	0.0018	0,004	629	1.35	8.7	22

Table 1 (continued)

Springs	Sampling date	Southing/Easting	Elevation (m)	T (°C)	Field pH	EC (μS/cm)	Na+ (mg/L)	K+	Ca²⁺	Mg²⁺	SiO₂	Fe²⁺/³⁺	Li⁺	B³⁺	As³⁺	Al³⁺	HCO₃⁻	SO₄²⁻	Cl⁻	Ionic Balance
Rambo 1–2007[e]	6/7/2006	523,058/9017886	1127	72	8.3	3700	806	83.4	10.5	7.9	–	–	0.758	2.87	0.1433	–	1760	139	181	0.96
Rambo 2–2007[e]	6/7/2006	523,026/9018021	1087	74.1	8.3	3700	821	83.5	15.9	8.5	–	0.03	0.751	2.84	0.1408	–	1730	138	180	3.8
Rambo 3–2007[e]	6/7/2006	522,965/9018008	1087	80.2	8.5	3800	818	82	17.1	8	–	0.177	0.762	2.88	0.1485	–	1760	143	184	0.9
Main spring 1–2007[e]	11/3/2006	520,022/9019159	1140	74	7.9	3830	802	102	21	16.2	–	0.024	0.725	2.46	0.1128	–	1880	146	175	4.1
Main spring 1–1998[g]	–	–	–	18	7.8	–	852	113	20	19.5	50	–	0.8	0.122	–	–	2067	163	199	0.5
Main spring 2–1998[g]	–	–	–	65	7.9	–	870	109	20	14.6	47.5	–	0.85	0.114	–	–	1924	165	227	1.5
Main spring 3–1998[g]	–	–	–	75	8.3	–	843	109	24.1	14.6	62.5	–	0.83	0.114	–	–	1828	164	223	2.7
Main spring 1985[d]	–	–	–	73	6.9	–	790	102	49	19	85	–	–	–	–	–	2770	160	184	14
Rambo 1–1978[h]	–	–	–	86	6.6	–	840	93	23	8	68	–	–	–	–	–	3580	170	215	25.6
Rambo 2–1978[h]	–	–	–	83	7	–	860	90	23	8.2	61	–	–	–	–	–	2580	165	220	11.6
Rambo 3–1978[h]	–	–	–	73	6.8	–	790	102	49	19	85	–	–	–	–	–	2870	160	184	15.4
Rambo 1970[f]	–	518,362/9019980	–	65	8.4	–	805	114	20	14.6	90	–	–	–	–	–	1721	163	223	2
Kaguri 1959[b]	Dec-55	–	–	66	8.4	2721	835	114	24.9	5.83	90.1	–	–	–	–	–	1818	163	223	1.8

Nd not detected; [a]Alexander et al. (2016); [b]James (1959); [c]Kraml et al. (2008); [d]Makundi and Kifua (1985); [e]Mnjokava (2007); [f]Nzaro (1970); [g]Pisarskii et al. (1998); [h]SWECO (1978)

Fig. 3 Geochemical modeling step using Phreeqc in Songwe geothermal area. **1a**–**c** are for the model at surface temperature, while 2**a**–**c** Are for the model at reservoir conditions
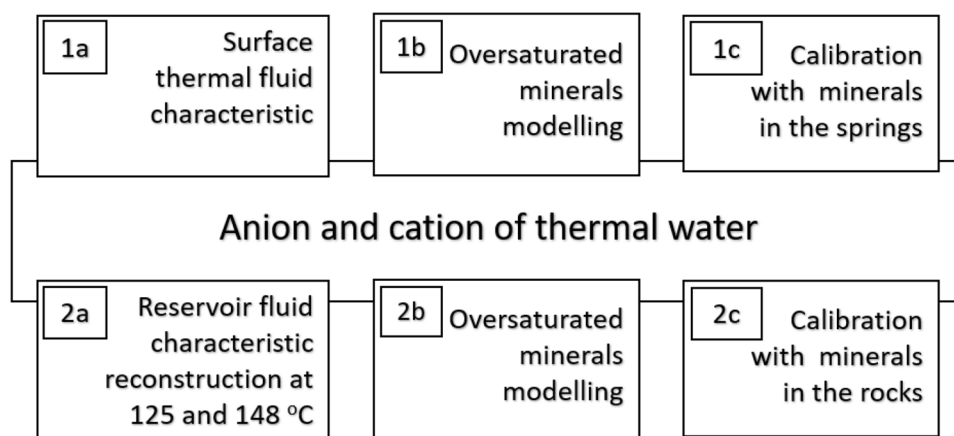

1a	Surface thermal fluid characteristic		1b	Oversaturated minerals modelling		1c	Calibration with minerals in the springs

Anion and cation of thermal water

2a	Reservoir fluid characteristic reconstruction at 125 and 148 °C		2b	Oversaturated minerals modelling		2c	Calibration with minerals in the rocks

Table 2 Mineral composition and rock physical properties of selected rock formations in the Songwe graben

Name	Mineral composition	Porosity [%]	Permeability [m^2]
Proterozoic Metamorphics	K-feldspar, Ca-Al-pyroxene, FCO$_3$-apatite, titanite, amphibole, quartz, albite, and hematite (data from this study and Alexander et al. 2016)	–	2.2–6.9×10^{-14} [a]
Permo-Triassic Karoo Group	Quartz, muscovite, illite/smectite, kaolinite, K-feldspars, epidote, zircon, kyanite, pyroxene, chlorite, amphibole, calcite, and hematite (data from this study; Dypvik et al. 1990; Wopfner and Kaaya 1991)	9.4–12.2 [a], 0.5–3.3 [c]	1.1×10^{-13}–1.3×10^{-12} [a]
Triassic Red Sandstone	Quartz, k-feldspar, muscovite, FCO$_3$-apatite, albite, nontronite-Ca, and nontronite-Na (data from this study; Alexander et al. 2016; Roberts et al. 2004)	15 – 21 [b]	8.4×10^{-13} [a]
Quaternary Volcanics	Quartz, albite, k-feldspar, illite, kaolinite, calcite, thenardite, Ca-Al-pyroxene, FCO$_3$-apatite, and amphibole (data from this study; Alexander et al. 2016; Mtelela et al. 2016)	–	–

[a]This study; [b]Beyer and Clutsom (1978); [c]Christopher (2015)

Surface rock samples

Rock samples were taken at areas of emerging thermal springs. To identify mineral compounds, the surface rock samples were analyzed by X-ray diffraction (XRD) (Bruker D8 Advance diffractometer, with Cu Kα radiation and a Bragg-Brentano geometry) at the S-Rat Facilities Group of Delft University of Technology. About 1 gr of sample powder was deposited in PMMA holder L25, measured through XRD between coupled θ–2θ scan 10°–110°, with a step size 0.030° 2θ, and counting time per step of 1 s. The data interpretation has been done using Bruker software DiffracSuite.EVA versus 5.2. The porosity of the samples is measured using a He-Pycnometer ("Ultra Pycnometer 1000"). The permeability was measured using a portable handheld air permeameter from NER (https://www.ner.com/site/systems/tinyperm3.html). A rubber nozzle is pressed against the sample and withdraws air from it. The air is pulled from the sample and a micro-controller unit simultaneously monitors the syringe volume and the transient vacuum pulse created at the sample surface.

Geochemical modeling

To understand the geothermal fluid source in the Songwe basin we used geochemical modelling using PHREEQC version 3.6.2 (Parkhurst et al. 2013) with the Lawrence Livermore National Laboratory aqueous model database (llnl.dat) according to the scheme in Fig. 3. We tested possible thermal water interaction with all lithologies of the study area at the surface temperature and reservoir temperature. First, for the reservoir temperature model, the hot spring composition was calculated back to a reservoir fluid composition using the steam fraction produced by boiling at two reservoir temperatures (125 °C and 148 °C) (Fig. 3). In surface temperature models we first used measured chemical concentrations of the springs. In a second step, thermal water in springs and/or the calculated reservoir water react with different rock types of the study area to simulate water-rock-interaction in this specific lithology at different temperatures. This is done to test if the resulting fluid composition and precipitating minerals match with the measured values. The reaction in the equilibrium model gives saturation indices (SI) for different minerals. A negative SI suggests dissolution of the
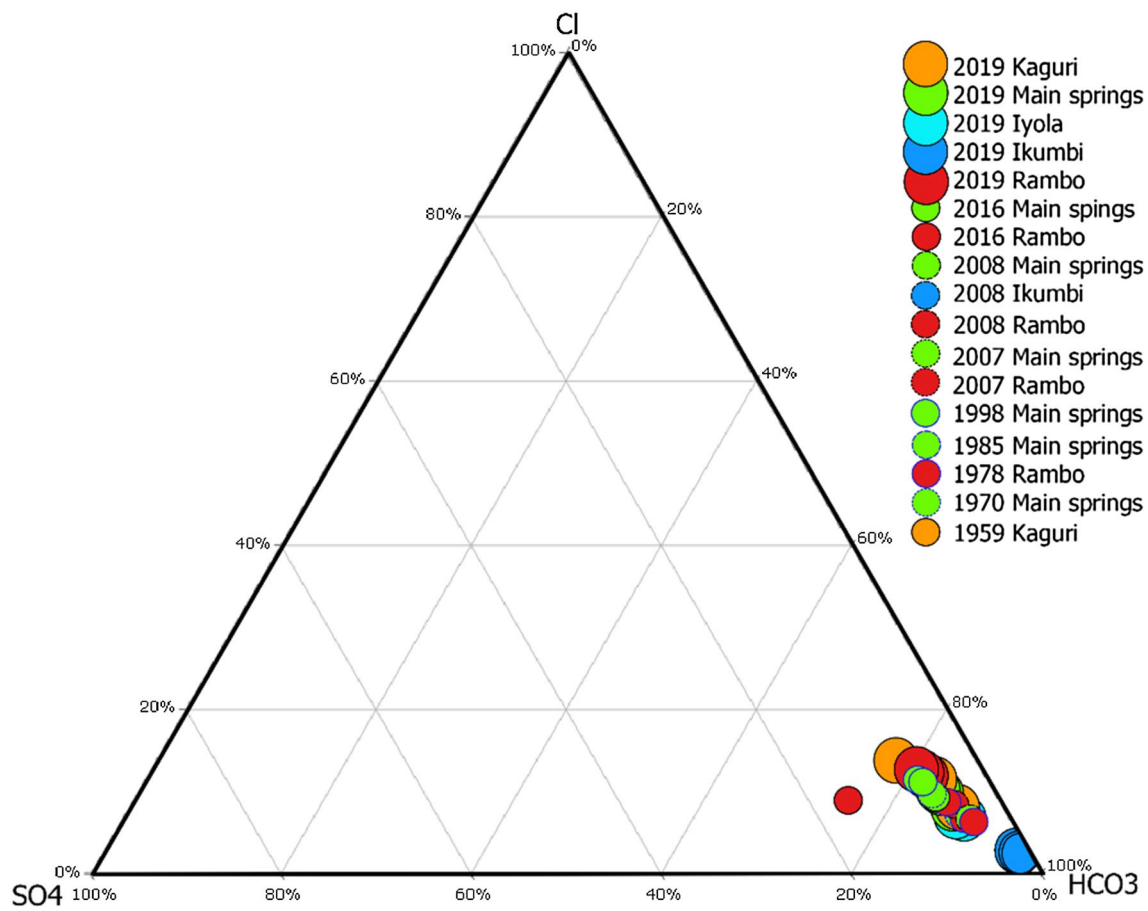
Fig. 4 Water type of thermal manifestations in the Songwe area from 1959 to 2019 based on anion concentrations

mineral while a positive SI suggests precipitation of the mineral (Brehme et al. 2016). Modelled precipitated minerals in the surface temperature were compared to observed precipitated minerals at the hot springs. In the reservoir temperature model, modelled precipitated minerals were compared to measured minerals in the rocks. The composition of the rock was taken from XRD data and literature (Table 2). The best match indicates the real water-rock interaction and marks the lithology where the geothermal fluid originates. Thus, the reaction model improves our understanding of the water-rock interaction in the geothermal system and indicates the geothermal fluid source in the Songwe basin.

Results

Thermal spring characterization

Songwe geothermal springs can be divided into five groups, based on their location: Iyola, Main springs, Kaguri, Rambo, and Ikumbi. Except Ikumbi springs, they are located along the Songwe river, at the west side of the Songwe graben. The

graben represents a NW-SE extended structure with a river and carbonate deposits surrounding the springs (Fig. 1). Iyola springs (62 to 74 °C) rise near to the river and from the river bed below the water with gas bubbles (Table 1). SW of Iyola and 50 m elevated, Main springs discharge from thick-blocky travertine rocks with temperatures of about 68 to 75 °C. In the western-central part of the Songwe graben, Rambo springs discharge with higher temperatures ranging between 70 and 83 °C also from travertine rocks. Kaguri springs discharge close to Rambo but at a lower elevation in the river bed with lower temperatures of 48 to 71 °C. Approximately ~6 km southeast of Rambo springs along the Ikumbi river, Ikumbi springs rise, with the lowest temperature of 37 to 44 °C in the study area. The most abundant rocks at Ikumbi springs are volcanic rocks.

The pH of the thermal springs is near neutral to slightly alkaline (5.8–8.3), except for 'Rambo new' spring which exhibits a slightly acidic pH (4.8) (Arnorsson et al. 1982; Reed and Nicolas 1984; Truesdell and Jones 1974; Wilson 1961). The electrical conductivity (EC) ranges from 410 to 3600 μS/cm in our measurements and 3830 μS/cm in former studies. The highest EC occurs in the Iyola springs (in
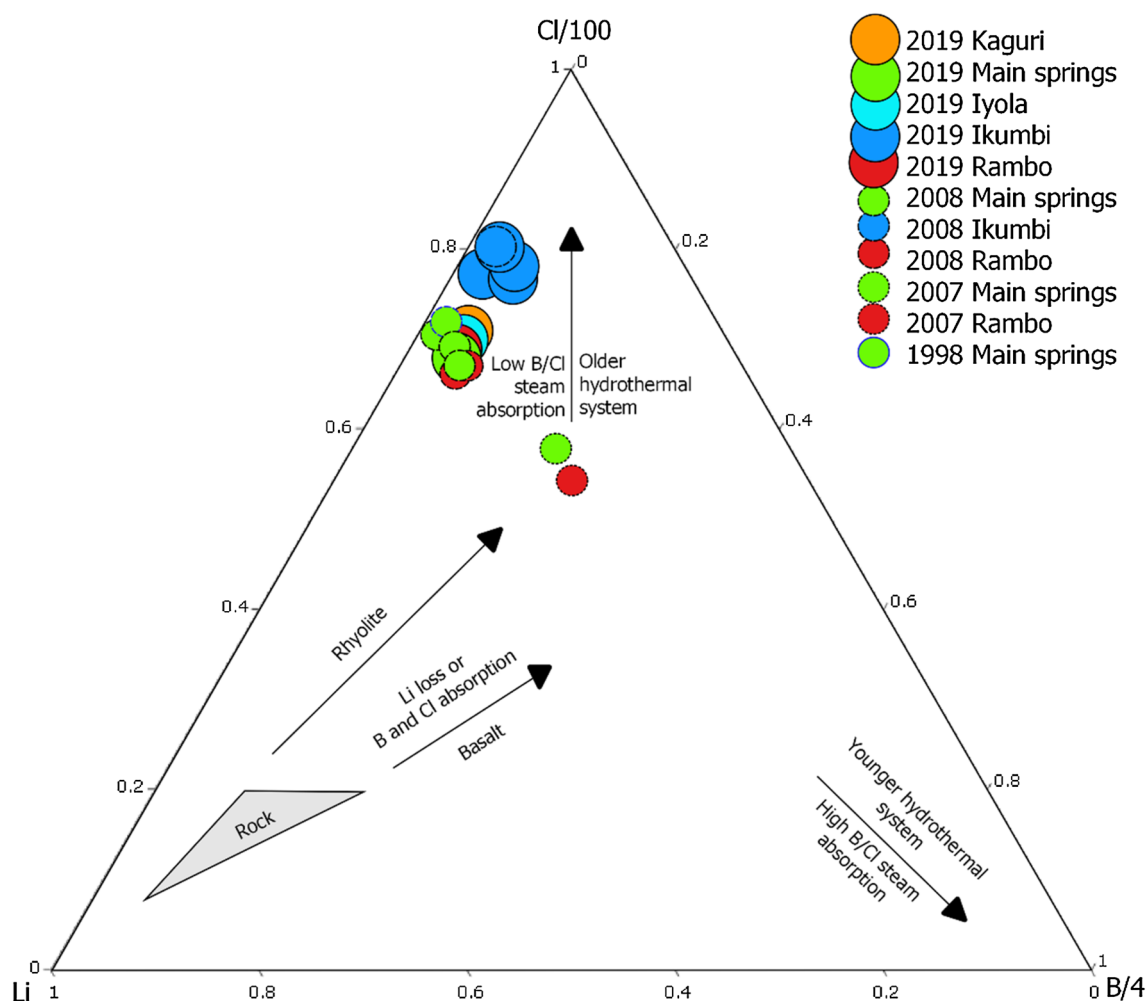
Fig. 5 Relative concentration of Li-Cl-B of Songwe thermal manifestations from 1998 to 2019

former studies in Main springs) with increased concentrations of all common ions, while Ikumbi springs show the lowest EC (Table 1).

The dominant anion in Songwe geothermal springs is HCO_3, ranging from 430 to 2248 mg/L in our measurements compared to up to 3580 mg/L in former studies. Also, the Cl-SO_4-HCO_3 triangular diagram (Fig. 4) shows, that all the springs plot in the HCO_3 apex. Interestingly, Ikumbi springs show high concentrations of SO_4 and Cl but contain the lowest absolute bicarbonate. Cl and SO_4 are the second most abundant anions with lower concentrations of 8 to 223 mg/L, and 5 to 178 mg/L (in former studies up to 227 and 430 mg/L), respectively. Cl concentrations appear within the range of common geothermal fluids of about <10 to 100,000 mg/kg (Nicholson 1993). The most dominant cations in the springs are Na with up to 980 mg/L, and K, Ca, Mg, Li and Fe, with lower concentration of 44–107 mg/L (formerly up to 114 mg/L), 12–61 mg/L

(formerly 10–49 mg/L), 5–24 mg/L (formerly 3–20 mg/L), 0.02–0.79 mg/L, and less than 0.02 mg/L (formerly up to 0.17 mg/L), respectively (Table 1). The low concentrations of these cations are common for geothermal fluids. In high temperature fluids, Ca and Mg typically occur at low levels of about < ~50 mg/kg and 0.01–0.1 mg/kg, respectively. (Nicholson 1993).

Rock composition

All geological layers have been observed during field work in 2019 mostly in unaltered conditions. XRD analysis show typical sandstone minerals for Karoo and Red Sandstone layers, e.g. quartz, feldspar and muscovite. Several minerals have been detected in the Karoo Sandstone as indicators for high-temperature fluid-rock interaction, e.g. illite, smectite and kaolinite (Table 1). Fractures, observed especially in Red Sandstone and Karoo Sandstone outcrops, were filled

**Table 3** Ratios of element concentrations in thermal manifestations in this study (2019)

Springs	Sampling date	Cl^-/B^{3+}	Cl^-/As^{3+}	Na^+/Mg^{2+}	Cl^-/Mg^{2+}
Rambo old	11/5/2019	108		116	19
Rambo middle	11/5/2019	110		118	20
Rambo new	11/5/2019	109		113	19
Kaguri 1	11/7/2019	111		108	18
Kaguri 2	11/7/2019	108		106	15
Kaguri 3	11/7/2019	112		111	18
Main spring 1	11/5/2019	103		64	10
Main spring 2	11/5/2019	104		58	9
Main spring 3	11/5/2019	105		56	8
Main spring 4	11/5/2019	104		47	7
Iyola 1	11/5/2019	109		36	5
Iyola 2	11/5/2019	111		41	6
Ikumbi 1	11/6/2019	246		26	1
Ikumbi 2	11/6/2019	605		20	1
Ikumbi 3	11/6/2019	616		22	1
Ikumbi 4	11/6/2019	121		24	1
Ikumbi 5	11/6/2019	89		23	1
Rambo 2016[a]	1/23/2016			256	46
Main spring 2016[a]	1/19/2016			50	9
Rambo 1-2008[c]	6/7/2006	76	2675	108	16
Rambo 2-2008[c]	6/7/2006	77	2610	108	16
Rambo 3-2008[c]	11/1/2006	90	4184	95	15
Rambo 4-2008[c]	6/7/2006	77	2698	102	15
Main spring 1–2008[c]	11/3/2006	86	3273	52	7
Main spring 2–2008[c]	6/27/2007	98	2871	53	9
Ikumbi 1-2008[c]	7/1/2007	543	11,553	18	1
Ikumbi 2-2008[c]	7/1/2007	19	10,566	25	1
Ikumbi 3-2008[c]	7/1/2007	19	10,963	19	1
Ikumbi 4-2008[c]	7/1/2007	19	10,214	22	1
Rambo 1-2007[e]	6/7/2006	22	2669	108	16
Rambo 2-2007[e]	6/7/2006	497	2702	102	15
Rambo 3-2007[e]	6/7/2006	607	2618	108	16
Main spring 1-2007[e]	11/3/2006	597	3279	52	7
Main spring 1-1998 [g]	–			46	7
Main spring 2-1998 [g]	–			63	17
Main spring 3-1998 [g]	–			61	10
Main spring 1985[d]	–			44	7
Rambo 1-1978 [h]	–			111	18
Rambo 2-1978 [h]	–			111	18
Rambo 3-1978 [h]	–			44	7
Rambo 1970[f]	–			93	17
Kaguri 1959[b]	Dec-55			151	26

Former studies from: [a]Alexander et al. (2016); [b]James (1959); [c]Kraml et al. (2008); [d]Makundi and Kifua (1985); [e]Mnjokava (2007); [f]Nzaro (1970); [g]Pisarskii et al. (1998); [h]SWECO (1978)

with carbonate minerals. They form ~20% of the rock volume. Effective porosity and specific permeability measured in the laboratory show low values of maximum 21% porosity for the Red Sandstones and a maximum permeability of 1.3×10^{-12} m^2 for Karoo Sandstones (Table 2). Geothermal manifestations mostly arise from travertines or Red Sandstone rocks, while Ikumbi springs are located within the Quaternary Volcanics in the east.

Fig. 6 Relative concentrations of Na–K-Mg of Songwe thermal manifestations from 1959 to 2019 plotted in the Giggenbach diagram for **a** high temperature systems (Giggenbach 1988a, b) and **b** lower temperature systems (< 200 °C) (Giggenbach and Soto 1992)
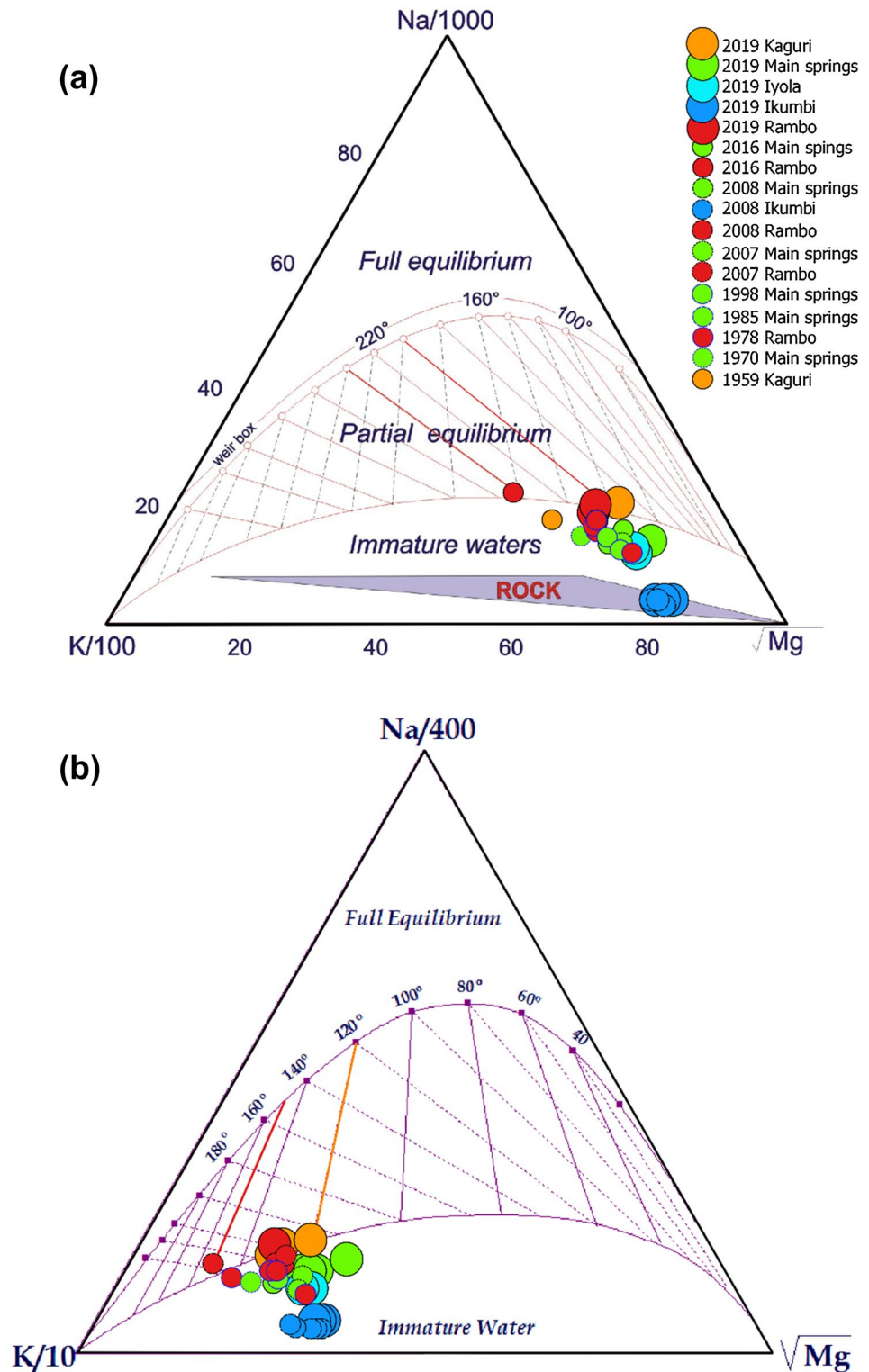
Element ratios in thermal waters

The relative concentrations of lithium, chlorite and boron of Songwe thermal springs are shown in Fig. 5. Most of Songwe thermal springs plot close to the Cl corner, near the

Cl-Li line and some close to older hydrothermal systems. Ikumbi springs show a slightly higher Cl relative to Li and B than other springs. All the springs plotting in Fig. 5 are consistent with the results of previous studies, except Rambo

and Main springs in 2007, which show a slight increase in B content.

The Cl/B ratios show different trends for Ikumbi springs (89–616) compared to the other Songwe springs (103–111). Ikumbi springs also have a higher Cl/As ratio compared to the other springs. Our study shows that Kaguri and Rambo springs have high Na/Mg (>100) and Cl/Mg ratios (>14), a similar value to that presented in previous studies (Table 3).

Geothermometry

Solute geothermometers use variations of element concentrations in hot springs as a function of temperature to calculate the temperature of a geothermal system. Geothermometers are based on several assumptions including full equilibration and no-mixing, which not always meet realistic conditions (Fournier 1977; Nicholson 1993). HCO_3-waters, for instance, are often considered to occur far from the reservoir as a result of steam heating and condensation. However, depending on the geological setting, they can also represent deep reservoir fluids in non-volcanic but high temperature systems such as in Turkey and Africa (Nicholson 1993). Therefore, the solute geothermometer calculations are still applied for Kaguri and Rambo springs, which have high surface temperatures, and high HCO_3 concentrations. Additionally, the Na-K-Mg ternary diagram is used to estimate reservoir temperatures and shows that Kaguri and Rambo springs are partially equilibrated waters, which allows using them for geothermometer calculations (Fig. 6).

In the Na-K-Mg diagram, Rambo shows a distinctive span of Na-K temperatures over the years (Fig. 6). Some samples plot in the range of 200 to 240 °C, exemplary for high-temperature systems, and some at 120 to 150 °C exemplary for low temperature systems. To clarify the appropriate Na-K temperature for the study area, the Na-K geothermometer proposed by Fournier (1977) and Giggenbach (1988a, b) is used. The results show that Kaguri and Rambo springs equilibrated at a subsurface temperature range of 216 to 232 °C (Table 4). Slightly higher temperatures have been proposed in previous studies: 217 to 256 °C for Rambo springs, 245 and 259 °C for Kaguri springs. The Na-K-Ca geothermometer also shows high temperatures of >200 °C (Table 3). A Mg correction for the Na-K-Ca geothermometer, because Mg is very high in the Songwe thermal springs (up to 18 mg/L), then gives lower temperatures of 116 to 142 °C. Likewise, the K-Mg geothermometer suggests lower temperatures (125–148 °C) assuming interfering fast kinetic reactions with K and Mg, thus a faster re-equilibrium of the fluid. The low temperatures estimated by previous studies is confirmed by SiO_2 quartz geothermometry results, which predict that Songwe fluids equilibrated at 113 to 128 °C (Table 3). Although the chalcedony geothermometer predicts even lower temperatures of 82 to 104 °C, the correlation of SiO_2 content and C_{2K}/C_{Mg} indicates that mostly Kaguri and Rambo thermal waters are in equilibrium with SiO_2 quartz (Fig. 7).

Mixing model

Geothermometer application for mixed thermal waters can influence the reliability of the estimated temperature. Thus, two mixing models were applied to evaluate the subsurface temperature of the Songwe area, estimated by solute geothermometers. Figure 8 shows the silica-enthalpy model (Truesdell and Jones 1974) for Rambo, Main springs, Kaguri and Ikumbi thermal springs. The mixing line is based on the sample with the highest and lowest silica content. The estimated temperature of the mixed thermal springs is between 100 °C and 124.5 °C based on the silica (chalcedony)-enthalpy mixing model, but the silica (quartz)-enthalpy mixing model shows higher temperature between 128.5 °C and 148.3 °C. The chlorite-enthalpy mixing model results in a temperature of 142.5 °C. Additionally, another evidence for mixing processes in our geothermal waters is shown by the relationship between Cl and conservative species B in Fig. 9. All the thermal springs show a linear relationship between Cl and B.

Reservoir fluid chemistry

The fluid characteristics for the reservoir temperature were reconstructed using one representative spring water composition out of each group: Rambo old, Kaguri 1, Main spring 2, Iyola 1 and Ikumbi 4. Concentrations of all species were calculated for 125 °C and 148 °C, representing the Songwe deep reservoir temperature, based on K-Mg geothermometer results. At these temperatures, it is assumed that the steam separates from the fluid phase during boiling and ascent to the surface. After the steam fraction is subtracted from the reservoir fluid, the liquid phase has a smaller mass and increased concentration of elements. Therefore, all solute concentrations of the reservoir fluid in Table 5 are lower than thermal springs at surface.

The pH of the reservoir fluid can be estimated using mineral equilibria reaction. Carbonate and especially calcite dissolution equilibria are commonly used to get a close approximation of the reservoir pH. First, carbonate equilibria are used in this study since Songwe thermal springs are dominated by bicarbonate evolving from the dissociation of dissolved carbon dioxide into bicarbonate and hydrogen in equilibrium governing described (Nicholson 1993):

Table 4 Estimation of reservoir temperature by different geothermometers for thermal manifestations in this study (2020) and former studies from: [a]Alexander et al., 2016; [b]James, 1959; [c]Kram et al., 2008; [d]Mjakava, 2007; [e]Nzaro, 1970 and [f]SWECO, 1978

Springs	SiO_2 Quartz (Fournier)	Chalcedony (Fournier)	Na–K (Giggenbach)	Na–K (Fournier)	Na–K-Ca	Na–K-Ca Mg correction	K-Mg
	°C						
Rambo old			227	211	209	137	125
Rambo middle			225	209	209	142	125
Rambo new			232	217	210	136	126
Kaguri 1			231	215	213	136	125
Kaguri 2			224	208	201	137	126
Kaguri 3			216	197	199	116	125
Rambo 2016[a]	113	84	256	243	224	163	148
Rambo 1–2008[c]	117	88	235	220	220	12	126
Rambo 2–2008[c]	118	90	233	217	213	24	125
Rambo 3–2008[c]	117	89	240	226	220	16	126
Rambo 4–2008[c]		89	234	219	215	15	125
Rambo 1–2007[d]			235	220	220	139	126
Rambo 2–2007[d]			234	219	215	134	125
Rambo 3–2007[d]			233	217	213	138	125
Rambo 1–1978[f]	117	88	241	226	216	49	129
Rambo 2–1978[f]	111	82	236	221	213	42	128
Rambo 3–1978[f]	128	101	254	240	216	− 23	119
Kaguri 1959[b]	128	104	259	245	229	113	141
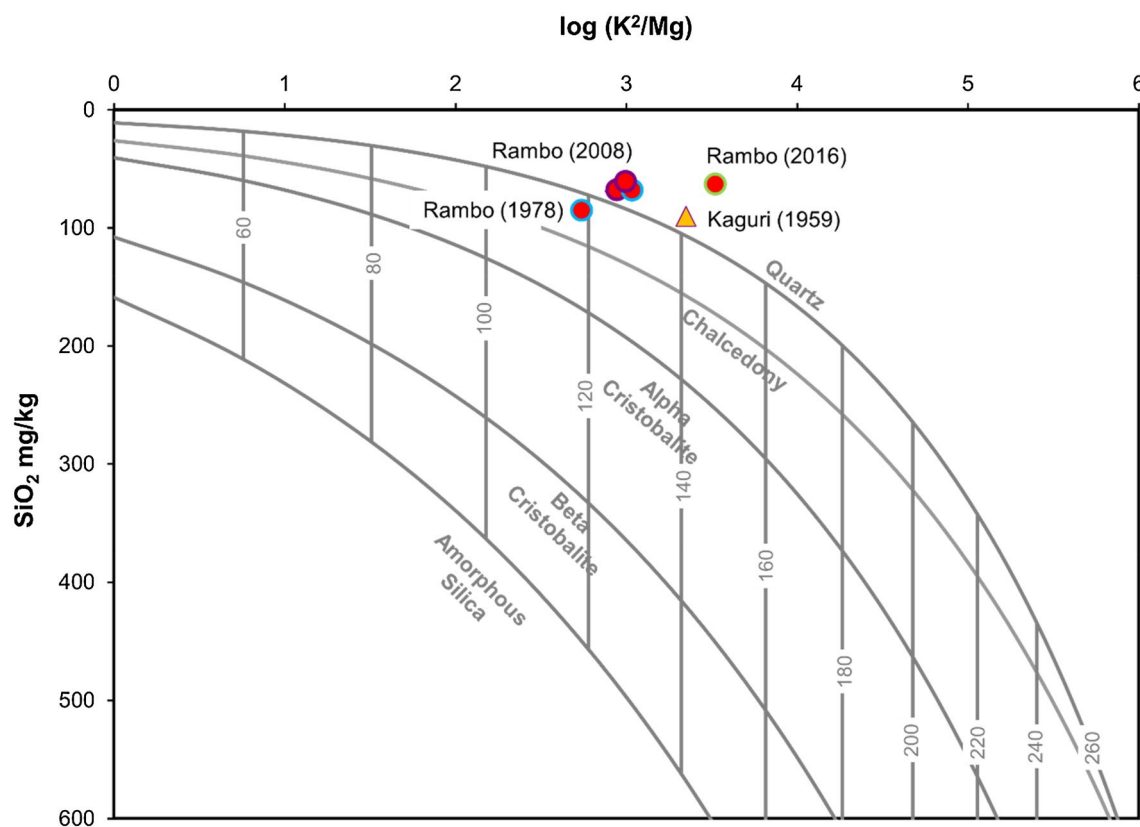
Fig. 7 Diagram of SiO_2 versus log K^2/Mg of Songwe thermal water, concentration in mg/l, based on Giggenbach and Soto (1992). The curves provide information on equilibrium attainment for SiO_2 and K-Mg geothermometers. Most thermal water plots near the quartz curve, except for Rambo (1978) which plots between quartz and chalcedony curve, suggesting that equilibria with quartz took place rather than with chalcedony
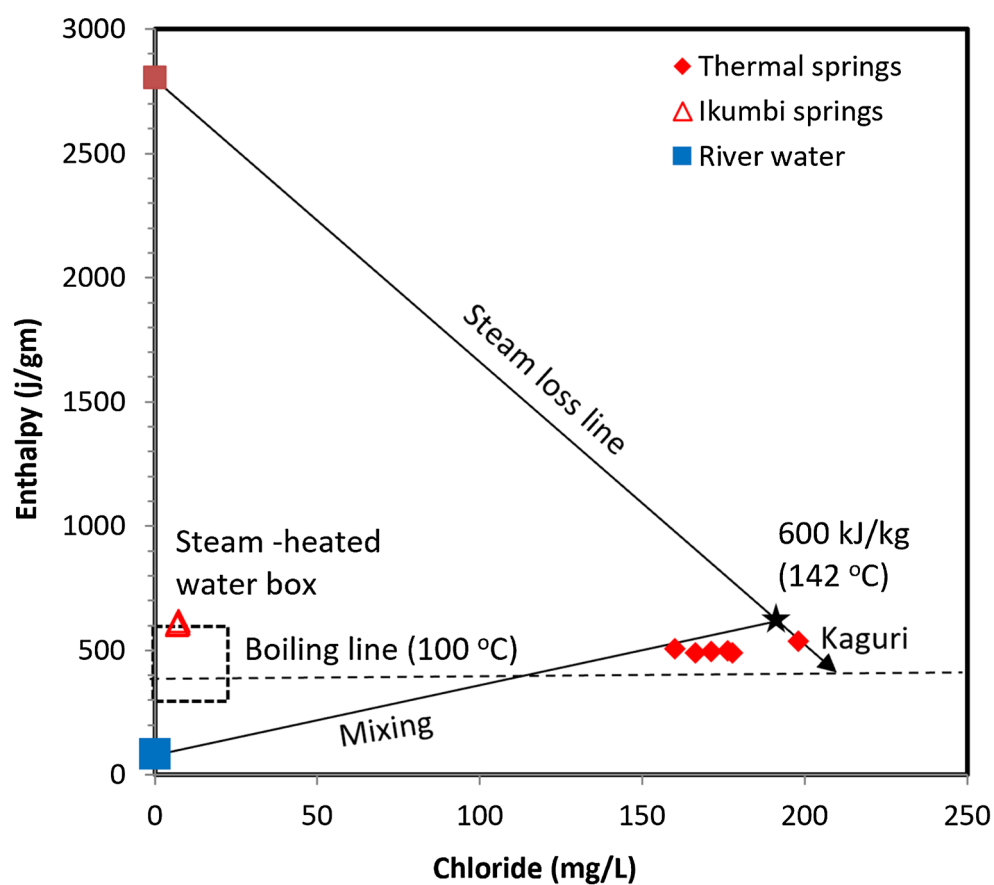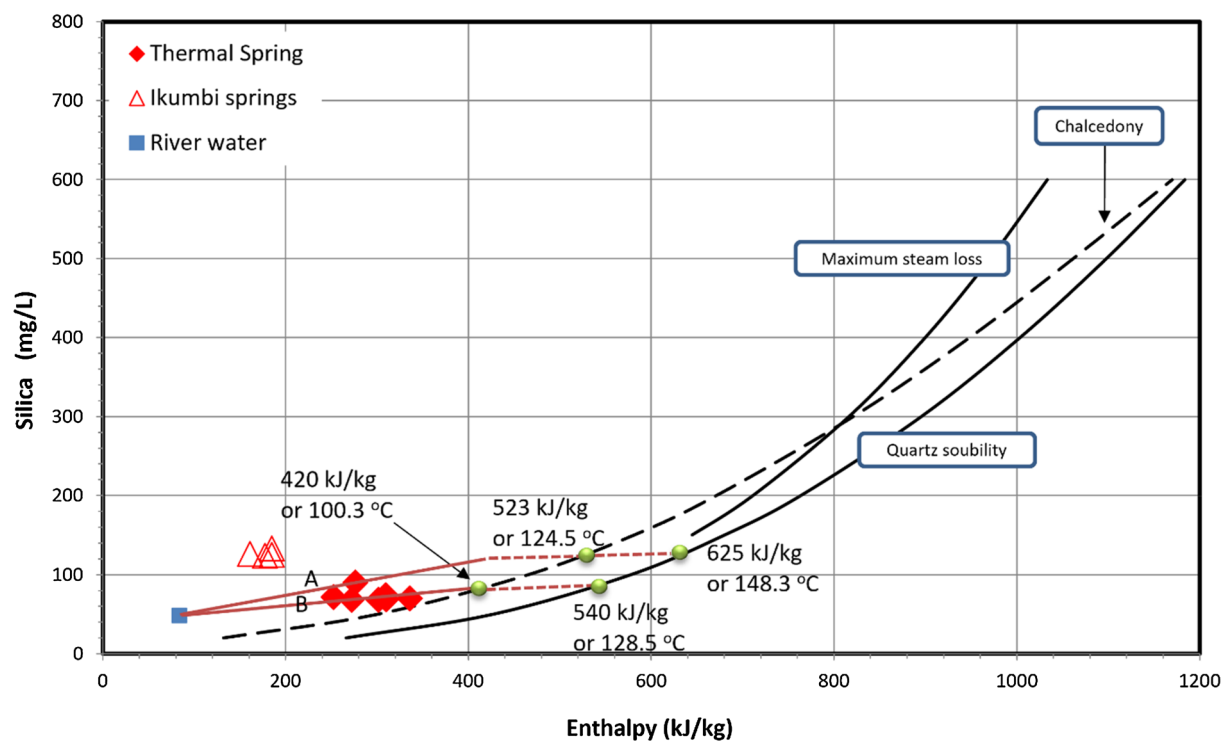
◀**Fig. 8** Mixing model of silica-enthalpy (based on chalcedony and quartz geothermometry temperature) and enthalpy-chloride (based on quartz geothermometry temperature). Silica concentration from previous geochemistry studies (see Table 1). The mixing lines on both diagrams are drawn from cold Songwe river water to the quartz solubility and to the steam line. Intersection points are based on the spring with higher concentration of silica (line A) and lower concentration (line B). Ikumbi springs were excluded from the mixing line because they were suspected as steam-heated waters

$$H_2CO_{3(aq)} = HCO_{3-(aq)} + H^+_{(aq)}$$

The XRD data of rock samples in all springs, also show calcite minerals, thus, we additionally applied the calcite dissolution equilibria. The calcite method gives a lower pH value (5.8–6.3) than the carbonate method (6.0–6.2, Table 5). The differences in pH from both methods are the consequence of carbonic species concentration in the sample. The pH also differs depending on temperature. For the calcite equilibria, the lower pH (5.8) occurs at 148 °C which increases with decreasing temperature (125 °C: 6.3). The bicarbonate method has a reverse trend. Based on the assumption that pH varies with temperature and a neutral pH 7 observed at surface, a pH of ~5.5 at higher reservoir temperatures at depth is expected (Nicholson 1993). In our case, the pH calculation with calcite dissolution equilibria shows more reliable results.

Mineral saturation indices

To calculate mineral saturation indices, the Phreeqc program (Parkhurst and Appelo, 2013) is used to identify possibly precipitating minerals, shown by positive saturation indices. Our model represents thermal water at surface temperature and at reservoir temperature reacting with different lithologies in the study area. Input data are thermal spring compositions and calculated reservoir fluid compositions at temperatures of 125 °C and 148 °C including pH, Na, K, Ca, Mg, Fe, HCO_3, SO_4, and Cl (Tables 1 and 5). The primary minerals of each lithology in the Songwe area are from XRD data of rock samples and literature (Table 2).

There are eight scenarios modelled for the hot spring cluster at surface conditions: scenario I-V for Rambo, Kaguri, Main springs, and Iyola, and scenario VI, VII and VIII for Ikumbi springs, including volcanics observed at shallow depth (Table 6). At reservoir conditions, scenario I-V were modelled for reservoir fluids reconstructed from all springs, but scenario VI-VIII for Ikumbi springs only. In scenario I and IV, the thermal water reacts with a single lithology (Metamorphic rocks or Red Sandstone). While in scenario II, III, V, VI, VII and VIII, a mixture of lithologies from oldest to youngest (Metamorphic, Karoo, Red Sandstone, Volcanic) reacts with the water simultaneously. The reaction delivers a new fluid composition and oversaturated minerals, which precipitate at reservoir depth. The results are then compared to sampled water and mineral compositions as calibration data, to test which rocks the reservoir water has been in contact with. The resulting oversaturated minerals were divided into groups: weathered volcanics, clays, apatites, weathered metamorphics, and hydrothermal minerals. Their exact saturation indices and abundance vary per scenario (Supplementary Material: Table S1a-e and S2a-h). In the surface temperature model, the modelled oversaturated minerals are compared to minerals encountered at the hot springs and the real hot spring water composition to understand reservoir water flow pathways and its interaction with rocks. In more detail, minerals precipitating at hot springs derive from dissolved solids in the reservoir water, attained through water-rock interaction at depth. Our model can show at which rock layer the finally precipitating minerals have been dissolved.

Surface temperature model

The output of the reaction between thermal springs at their surface temperature with Metamorphics (scenario I) is dominated by weathered metamorphics with up to 19.5 SI in Kaguri, while the lowest SI is observed in Main springs (Supplementary Material: Table S1a). The second-highest SI values appear for apatites, while the lowest appear for carbonates and only in Kaguri (SI ~ 1).

Scenario II involves the reaction between water, Metamorphic and Karoo rocks and shows that Rambo shows the highest SIs in all mineral groups, but no spring shows a supersaturation of carbonates (Supplementary Material: Table S1.b). SIs of around 1 to 3 are observed for clays and weathered metamorphics in all other springs. Apatite, clays and metamorphics show especially high SIs of 12-18 in Rambo.

In scenario III, clays show again the highest variety of supersaturated minerals (Supplementary Material: Table S1.c). Weathered metamorphics show the highest SIs of 10-12. Also, hydrothermal minerals show high SIs of 11-12, besides in Kaguri. Only Kaguri and Main springs show carbonates as supersaturated.

Scenario IV model results (Supplementary Material: Table S1.d) show clay minerals with the highest variety and highest SIs of supersaturated minerals for the reaction of water with Red Sandstone. The second highest SIs occur for weathered metamorphics in all springs. All springs also show a supersaturation of carbonates, especially for the first time all thermal spring waters are supersaturated with aragonite and calcites.

The reaction of thermal waters with all lithologies in scenario V (Supplementary Material: Table S1.e) shows similar SIs for all springs. Clays are still the minerals with the highest variety. Highest SIs occur for weathered metamorphics

Fig. 9 Linear relationship between Cl and B of Songwe thermal springs
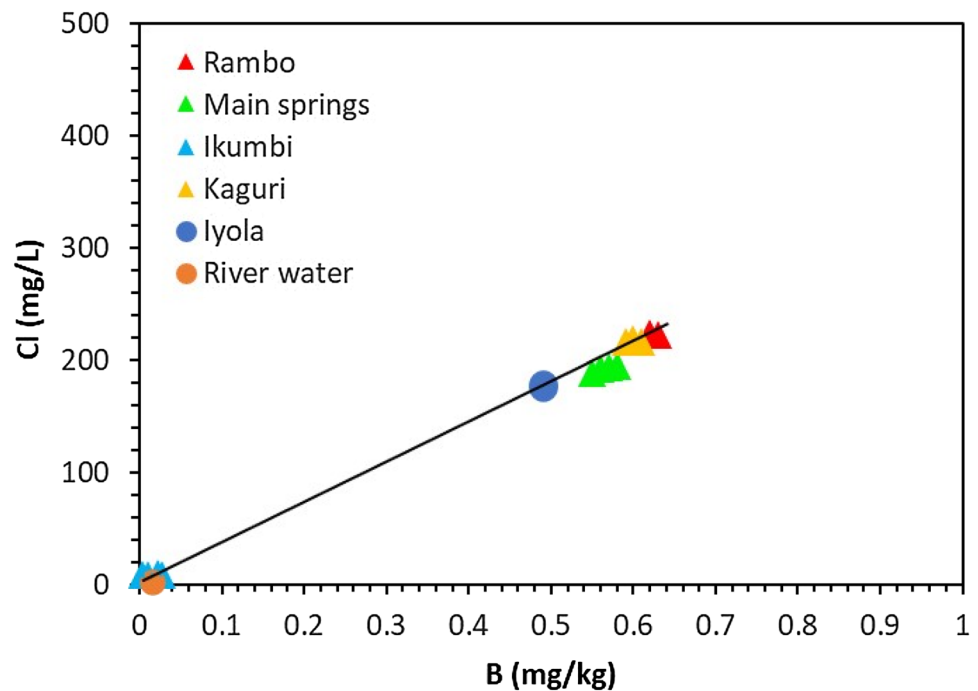
and hydrothermal minerals. Carbonates show the lowest SIs and do not precipitate in Rambo springs.

The reaction between all lithologies and thermal water is only modelled for Ikumbi (scenario VI, Supplementary Material: Table S1.f). Highest SIs of 10-15 appear for clays, carbonates, weathered metamorphics and hydrothermal minerals. The lowest SIs occur for clays. Muscovite is observed to be supersaturated and also observed at surface close to the spring.

Reservoir temperature model

The model results show that in scenario I (Supplementary Material: Table S2.a), most supersaturated minerals are weathered metamorphics, followed by clays and weathered volcanics. For weathered metamorphics and clays the SIs tend to be higher at 148 °C, while they tend to be lower for weathered volcanics at higher temperatures. The highest SIs appear for weathered metamorphics with several values of 10–20. Clays show SIs of ~12 and weathered volcanics mostly of 1–8. The water-rock reactions in scenario I involve metamorphic rocks as the only input, a possible reason for the high abundance of weathered metamorphics in the model outcome.

Scenario II model results (Supplementary Material: Table S2.b) show the highest variety in supersaturated clay minerals. However, their SIs are mostly around 1 with increased values at higher temperatures. The highest SIs of 4–11 occur for apatites, that are also observed at the hot springs. Weathered volcanics precipitate at all springs beside

Rambo, while weathered metamorphics are supersaturated at all springs. These different trends between the springs, are due to a higher variety in mineral composition in scenario II, representing metamorphics and Karoo.

The reactions at 125 and 148 °C in scenario III also show the clay minerals group as the most varying minerals with SIs around 8 (Supplementary Material: Table S2.c). The least supersaturated minerals are weathered volcanics and carbonates. Apatite and hydrothermal minerals show high SIs of 6-15 and is also found as surface mineral at the springs.

In scenario IV, clay minerals are still showing the highest variety and SIs of 2–12 with the highest values at Ikumbi (Supplementary Material: Table S2.d). The SIs decrease with increasing temperature. Carbonates are supersaturated in all springs with SIs around 1–3 and especially Calcite is also found as surface mineral at the springs. Apatites show higher SIs of 5–13 with increasing supersaturation at increasing temperature. Weathered metamorphics and volcanics are less abundant.

In accordance with other scenarios, scenario V shows at both temperatures of 125 °C and 148 °C, clays minerals as the varying mineral group with SIs of 1–10 (Supplementary Material: Table S2.e). Smectite is supersaturated in Rambo, Main springs, Iyola and Ikumbi (125 °C). Carbonates precipitate mainly in Kaguri, and a little bit in Iyola and Ikumbi springs. Calcite has also been observed onsite at the hot spring locations. Apatites are supersaturated in all springs with SIs of 6–19 and also observed as minerals at the locations. Weathered metamorphics, volcanics and hydrothermal

minerals occur at single hot springs with lower SIs of 1–8 mainly. Clays show higher SIs, while carbonates and apatites show lower SIs at increased temperature. The enrichment of clay minerals is also visible in decreasing K in the thermal springs in 2019 and the K uptake in secondary clays seen in the K-Na-Mg-Ca diagram (Fig. 10).

Scenario VI, VII and VIII results show a strong supersaturation of weathered volcanics at both 125 °C and 148 °C (Supplementary Material: Table S2.f, S2.g, and S2.h). In scenario VI also clays and apatites are supersaturated as well as found at the thermal springs. Scenario VII and VIII show less minerals supersaturated but high SIs of 10-18 for weathered volcanics and apatites. Lower SIs of 1-6 are found for clay minerals.

Discussion

Hydrogeochemistry

The results show that all the thermal springs in the Songwe area have a Na-HCO_3 water type. This is related to the presence of bicarbonate in the reservoir rocks. At Ikumbi springs located within volcanic rocks, the HCO_3 can also form near surface when CO_2 gas and steam condenses into cold water (steam heated water). The enthalpy-chloride model also shows that Ikumbi thermal waters plot in the steam heated water area (Fig. 8).

Kaguri, Rambo, Main springs, Iyola and Ikumbi have a similar water type, but different fluid pathways or a change of lithology at depth, shown by different element ratios. Element ratios can be used to identify the common source of reservoir fluids and identify physicochemical processes in a geothermal system (Nicholson 1993). Relatively high Na/Mg and Cl/Mg ratios are typical for high temperature fluids, that reach the surface rapidly defining the upflow zone of the system (Nicholson 1993). The ratios suggest that Kaguri and Rambo are situated in the upflow zone and are directly fed from the reservoir. This is in good agreement with high surface temperatures observed in both springs. Thus, Songwe thermal springs form a geothermal area with an independent geothermal (heat) source and are not an outflow of the Ngozi volcanic geothermal system as suggested by previous studies (GEOTHERM; Delvaux et al. 2010). During their rise to the surface, there is a chance that Songwe springs might mix with cold groundwater in the upflow zone as seen in Fig. 9 that shows a linear relationship between Cl and B. As a conservative species in geothermal fluids, Cl content will increase continuously during progressive water–rock interaction.

The alkali metal Li, which is least affected by secondary absorption processes, is typically used together with conservative elements B and Cl for evaluating a possible origin of geothermal fluids (Giggenbach and Soto 1992). Our results suggest that Songwe thermal springs were formed through absorption processes with low B/Cl magmatic vapor input and originate from an older hydrothermal system. Tritium data (Kraml et al. 2008) have been used to explain that Songwe thermal springs have very low (0.00 ± 0.02) tritium, suggesting relatively high residence times in the subsurface.

Reservoir temperature estimation

Classical geothermometers have been applied to Songwe geothermal springs which yield a wide range of temperatures from previous geochemistry studies. Makundi and Kifua (1985) argued that as part of the Mbeya volcanic area, Songwe is a high enthalpy system with temperatures of 217 °C based on the Na–K-Ca geothermometer. However, the Na–K-Ca geothermometer shows unreliable high temperatures because it is applied to HCO_3 waters in a low temperature system (Pope et al., 1987). Likewise, this study shows overestimated Na–K geothermometer results because of Kaguri and Rambo springs not being fully equilibrated and kinetic reactions including Na and K causing a slow re-equilibration (Fig. 6; Giggenbach 1988a, b; Hochstein 1988). In contrast, this study suggests that Songwe is a low to medium enthalpy geothermal system. K-Mg geothermometers and Na–K-Ca$_{(Mg\ correction)}$ (Table 4) give reasonable approximations of reservoir temperatures in the range of 125 to 148 °C. This is in good agreement with Alexander et al. (2016) who also predicted lower temperatures (112 ± 16 °C) based on K-Mg, Silica and quartz geothermometers.

The silica-enthalpy and enthalpy-chloride mixing models show that the temperature of possible parent fluid in the study area are in the range of 100 to 149.5 °C. Those numbers are higher than those obtained by the quartz geothermometer (Fig. 8 and Table 3), which suggests that most of the hot water is mixing with cooler water from shallow aquifers and/or that conductive cooling takes place during the ascent of the geothermal fluid to the surface.

Water–rock interaction modeling

Each of our hydrogeochemical models results in possibly precipitating mineral groups, while percentage and composition differ. A comparison with the mineral composition of the reservoir rocks and minerals precipitated at surface we obtained best fits of our models. The best fitting scenarios are summarized in Fig. 11, including saturation indices and percentages. Lithologies are shown in coloured layers including porosity and permeability values. Arrows show the reaction pathway, covering reactions with 1–3 layers and

Table 5 Estimated chemical composition of reservoir fluid at 125 °C and 148 °C based on the chemical concentration of thermal springs using steam fraction calculation, K-Mg geothermometer and calcite dissolution equilibria calculation for pH

Springs	T surfaces (°C)	pH springs in the field	T Reservoir (°C)	Steam fraction	pH (H_2CO_3)	pH ($CaCO_3$)	Na^+ mg/L	K^+	Ca^{2+}	Mg^{2+}	$Fe^{2+/3+}$	HCO_3^-	SO_4^{2-}	Cl^-
Rambo old	82.7	6.5	125	0.08	6.1	6.1	800.3	74.8	17.5	7.3	0.0029	1688.7	163.10	205.3
			148	0.12	6.0	6.2	763.1	71.3	16.7	6.9	0.0027	1610.3	155.5	195.8
Kaguri 1	70.9	8.6	125	0.10	6.1	6.0	782.8	76.8	15.3	7.6	0.0061	1464.1	159	197.2
			148	0.14	6.0	6.0	746.1	73.2	14.6	7.3	0.0058	1395.4	151.6	187.9
Main spring 2	75.5	6.2	125	0.09	6.0	6.1	739.7	79.6	33.7	13.6	0.0042	1759.7	156.4	176.3
			148	0.13	5.8	6.2	714.7	75.9	32.1	12.9	0.0040	1677.6	149.1	168.1
Iyola 1	74.4	6.8	125	0.09	5.9	6.1	742.8	97.2	55.4	21.5	0.0066	1966.8	153.3	159.6
			148	0.13	5.7	6.2	708	92.6	52.8	20.5	0.0063	1874.8	146.1	152.1
Ikumbi 4	41.3	7.9	125	0.15	6.4	6.1	103.2	39.3	11.9	4.5	0.0015	374.67	4.7	6.9
			148	0.19	6.3	6.2	98.2	37.5	11.4	4.3	0.0015	356.7	4.5	6.6

resulting saturation indices. The highlighted minerals in blue and yellow correlate with the observed minerals at each thermal spring. Figure 11a focuses on carbonate precipitation, Fig. 11b also shows other precipitating minerals at surface temperature. At Rambo, Kaguri, Iyola, and Main springs only carbonate minerals were detected at surface, while at Ikumbi mainly analcime, muscovite, and smectite have been detected. The best fitting model, showing carbonate precipitation in the model and in real case at Rambo, Iyola, Kaguri, and Main springs is when the fluid reacts only with Red sandstone (scenario IV). For Ikumbi, scenario VI (reaction with Metamorphics, Karoo, Red Sandstone and Volcanics) results in the best fit. Figure 11b presents the final results of the model, showing that Iyola, Main springs, Kaguri and Rambo spring water is mainly dissolving minerals from the Red Sandstone, resulting in massive carbonate precipitation at surface. Also, Ikumbi waters have been in contact with all lithologies, resulting in the precipitation of Analcime, Chabazie-Ca, Muscovite, and Smectite. Figure 11c, d show the reaction results at reservoir condition. The precipitation of measured minerals is only found in modelled reactions of scenario II, III and V for Iyola, Main springs, Kaguri and Rambo and scenario III, IV, VI, VII and VIII for Ikumbi. The best fitting model for Rambo, Iyola, Kaguri and Main springs at 125 °C and 148 °C is when the reaction involves the fluid, Karoo and Red sandstone (scenario III). It shows most secondary minerals precipitating (group of apatites, clays and hydrothermal minerals) in the modelled reaction and the measured minerals. Scenario VI is the best fitting model for Ikumbi where the group of apatites, clays and weathered volcanics precipitate in the modelled reaction confirmed by measured data. This is consistent with the Li-Cl-B data of Ikumbi (Fig. 5) that show a slightly higher Cl content relative to Li and B in other springs indicating that Ikumbi migrated from fluid in the old basement rock.

Conceptual fluid flow model

Integrating all data from this and former studies are summarized in a conceptual fluid flow model for the Songwe basin. Generally, faults and fractures control the fluid flow in the regional setting of the NW trending basin. Recharge happens most probably through the higher elevations NE of the Mbeya fault (Alexander et al. 2016). Meteoric water infiltrates here and mixes with deep hot fluids originating from the 40-km thick crust beneath the Songwe basin Kraml et al. (2008). This water is stored mainly in the metamorphic basement and ascends through faults and fractures in the basin. Water-rock interaction during the rise leads to secondary hydrogeochemical processes that change the chemical composition of thermal water.

Both models suggest that during ascension, fluids reach more permeable lithologies like the Karoo and Red

Table 6 Scenario reactions for modelling the fluid-rock interactions in Songwe geothermal area

Lithology	Mineral composition (input)	Scenario								The calibration minerals	
		Scenario I	Scenario II	Scenario III	Scenario IV	Scenario V	Scenario VI	Scenario VII	Scenario VIII	T surface	T Reservoir
Proterozoic Metamorphics	K-feldspar, Ca-Al-pyroxene, FCO_3-apatite, titanite, amphibole, quartz, albite, and hematite (data from this study and Alexander et al. 2016)	Thermal water + Metamorphics	Thermal water + Metamorphics and Karoo			Thermal water + Metamorphics, Karoo and Red Sandstone	Thermal water + Metamorphics, Karoo, Red Sandstone and Volcanics			Calcite and aragonite	Apatite
Permo-Triassic Karoo Group	Quartz, muscovite, illite/smectite, kaolinite, K-feldspars, epidote, zircon, kyanite, pyroxene, chlorite, amphibole, calcite, and hematite (data from this study; Dypvik et al. 1990; Wopfner and Kaaya 1991)			Thermal water + Karoo and Red Sandstone				Thermal water + Karoo, Red Sandstone and Volcanics			Illite, smectite, kaolinite, chlorite, calcite
Triassic Red Sandstone	Quartz, k-feldspar, muscovite, FCO_3-apatite, albite, nontronite-Ca, and nontronite-Na (data from this study; Alexander et al. 2016; Roberts et al. 2004)				Thermal water + Red Sandstone				Thermal water + Red Sandstone and Volcanics	Apatite, nontronite	
Quaternary Volcanics	Quartz, albite, k-feldspar, illite, kaolinite, calcite, thenardite, Ca-Al-pyroxene, FCO3-apatite, and amphibole (data from this study; Alexander et al. 2016; Mtelela et al. 2016)									Analcime. Chabazite-Ca, Muscovite, Smectite	Illite, kaolinite, calcite, thernadite, apatite

Fig. 10 The plot of weight-fractions of 10 K/(10 K + Na) and 10 Mg/(10 Mg + Ca) adapted from Giggenbach (1988a), b for thermal waters in Songwe. The diagram represents also general processes including water equilibrium with average crustal rocks along the "full equilibrium" line; "rock dissolution" as isochemical dissolution of crustal rocks (Giggenbach 1988a, b); and water mixing with seawater. None of Songwe thermal springs plot close to full equilibrium line
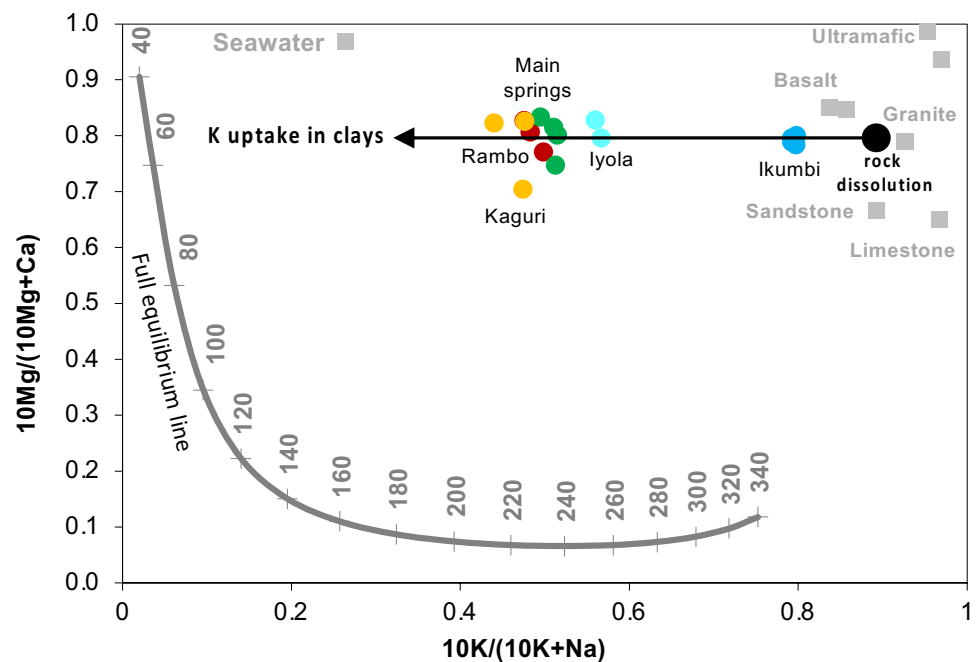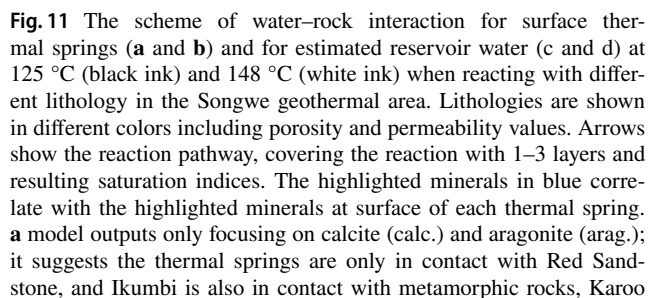

Sandstones. Due to higher permeability fluids now also percolate laterally within the sandstones and have a longer reaction time with these carbonate rich rocks. They eventually rise towards the surface at minor fracture sets, as observed at Rambo, Kaguri, Main springs and Iyola. Ikumbi water additionally is in contact with volcanic rocks overlaying the sandstones. Both hydrochemical models, calibrated with reservoir or surface temperature show, that these fluids are dominated by water-rock-interaction in the Red sandstone (Fig. 12).

During ascent of the fluids, temperature and pressure drops, resulting in cooling and degassing of CO_2. Degassing results in decreased solubility of HCO_3 and calcite/aragonite oversaturation, causing massive travertine deposits. High HCO_3 and Na concentrations in all spring waters support the theory of carbonate dissolution from the Red sandstone layer as the most common water-rock interaction in the Songwe basin.

Conventional geothermometry predicts reservoir temperatures in the range of 125 to 148 °C. The hydrochemical model at reservoir condition shows that thermal fluids react with Karoo and Red sandstone in the study area. The higher the reservoir temperature, the deeper the lithology in contact with thermal fluids.

Conclusion

This study presents a fluid source model of the Songwe geothermal system using data on the composition of thermal spring fluids, primary minerals of lithologies, and a water–rock reaction model. The medium to high temperature thermal waters of neutral pH and Na-HCO_3 type are driven by advective flow through interconnected fault/fracture networks. Fluid-rock interaction within permeable zones causes re-equilibrium of fluids with rocks, in fast kinetic reactions of mainly Mg with K, as well as Na and Ca with Mg correction. The K-Mg and Na–K-Ca (Mg correction) geothermometer shows an equilibrium temperature for the reservoir fluid between 125 and 148 °C. The reconstruction of the chemical fluid composition under reservoir condition and at surface temperatures are used to identify water–rock reaction scenarios most suitable for mimicking measured minerals in the rocks and for imitating minerals precipitating at the surface (i.e. calcite, aragonite, analcime, muscovite, and smectite). There are three best fitting reaction scenarios for fluid-rock interaction for different conditions and it can be used to identify the thermal water source: scenario IV for Kaguri, Rambo, Iyola, and Main springs, at surface temperature and scenario III at reservoir temperature and scenario VI for Ikumbi springs at both conditions. The thermal springs have been in contact with Red sandstone only at surface temperature, but at the higher temperatures, thermal water also reacts with deeper lithologies like Karoo and Red sandstone. Ikumbi is in contact with all lithologies including Younger Volcanics. These results are supported by relatively high Na/Mg and Cl/Mg ratios at Rambo and Kaguri, as well as

Fig. 11 The scheme of water–rock interaction for surface thermal springs (**a** and **b**) and for estimated reservoir water (c and d) at 125 °C (black ink) and 148 °C (white ink) when reacting with different lithology in the Songwe geothermal area. Lithologies are shown in different colors including porosity and permeability values. Arrows show the reaction pathway, covering the reaction with 1–3 layers and resulting saturation indices. The highlighted minerals in blue correlate with the highlighted minerals at surface of each thermal spring. **a** model outputs only focusing on calcite (calc.) and aragonite (arag.); it suggests the thermal springs are only in contact with Red Sandstone, and Ikumbi is also in contact with metamorphic rocks, Karoo

group (longest arrow) and younger volcanics. Ikumbi springs react with all lithologies in the Songwe field, supported by the precipitation of analcime, muscovite and smectite. **b** model outputs including all mineral groups: Apt (apatite), Car (carbonates), Clay, WM (weathered metamorphics), and WV (weathered volcanics). **c** model outputs focusing on minerals measured and precipitated in the model reactions consisting of HAp (Hydroxyapatite), FAp (Flouroapatite), Illite, Smec (smectite). Cl (chlorite), Non-Ca (nontronite-Ca), Non-Na (nontronite-Na), Cal (calcite) and Kao (Kaolinite). **d** model outputs of mineral groups percentage for the best fitting scenario. [a]This study; [b]Beyer and Clutsom ([1978](#))

(d)
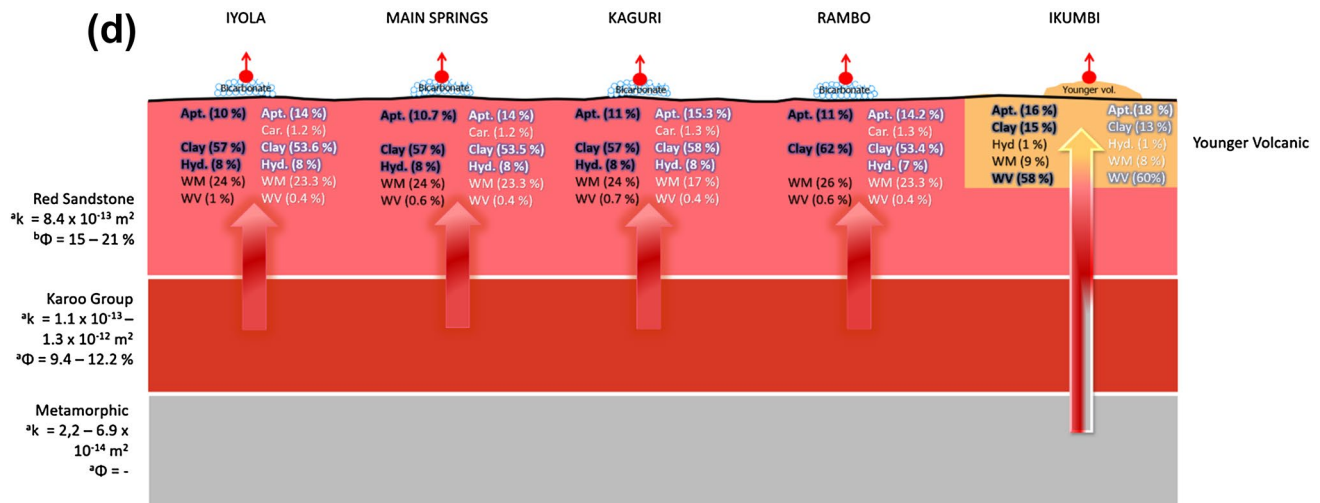
Fig. 11 (continued)
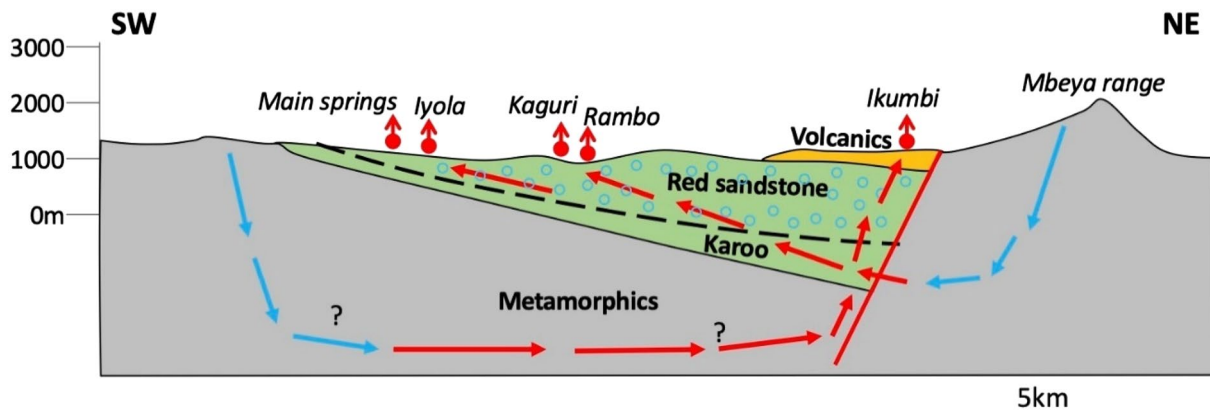
Fig. 12 Conceptual fluid flow model of the Songwe area after hydrogeochemical model interpretation. Showing fluid infiltration in the NE and supposedly SW, fluids rising along the fault and percolating within the sandstones before discharging in hot springs (Christopher 2015)

partial equilibration of thermal spring water, which suggests that Rambo and Kaguri are directly fed from the reservoir and located in the upflow zone of the Songwe geothermal system. The other springs are located at the outflow zone, which is generally controlled by NW–SE trending faults and fractures.

Autor contribution S.N.A. performed data interpretation, modelling, and drafted the manuscript with input from all of the authors. M.N., M.B. and E.M. conducted field work. S.J. and A.M. provided previous geochemical data; M.B and G.B. acquired the funding and supervised the research. All together approved the final form of the manuscript.

Declarations

Conflict of interest The authors report no competing interests.

References

Alexander K, Cumming W, Marini L (2016) Geothermal resource assessment report: Ngozi and Songwe Geothermal Prospects, Tanzania, Final Report dated September 2016 to UNEP/ARGeo and TGDC.

Arnorsson S, Sigurdsson S, Svavarsson H (1982) The chemistry of geothermal waterS in Iceland. I. Calculation of aqueous speciation from 0° to 370°C. Geochim Cosmochim Acta 46:1513–1532

Beyer LA, Clutsom FG (1978) Density and porosity of oil reservoirs and overlying formations from borehole gravity measurements Gebo Oil Field, Hot Springs County, Wyoming. Oil Gas Invest Chart. https://doi.org/10.3133/oc88

Brehme M, Scheytt T, Çelik M, Dokuz UE (2010) Hydrochemical characterisation of ground and surface water at Dörtyol/Hatay/Turkey. Environ Earth Sci 63:1395–1408. https://doi.org/10.1007/s12665-010-0810-1

Brehme M, Deon F, Haase C, Wiegand B, Kamah Y, Sauter M, Regenspurg S (2016) Fault controlled geochemical properties in Lahendong geothermal reservoir Indonesia. Grundwasser 21:29–41. https://doi.org/10.1007/s00767-015-0313-9

Brehme M, Regenspurg S, Leary P, Bulut F, Milsch H, Petrauskas S, Valickas R, Blöcher G (2018) Injection-triggered occlusion of flow pathways in geothermal operations. Geofluids 2018:4694829. https://doi.org/10.1155/2018/4694829

Brehme M, Giese R, Dokuz UE, Bulut F (2021) Fluid pathways identified beneath Narlı Lake (Central Anatolia) show the geothermal potential of former volcanoes. Sci Rep 11(1):1–8

Christopher B (2015) Geological and geophysical investigation of the southeastern Karoo basin. University of Fort Hare, South Africa, South Africa

Delvaux D, Kraml M, Sierralta M, Wittenberg A, Mayalla JW, Kabaka K, Makene C (2010) surface exploration of a viable geothermal resource in Mbeya Area, Sw Tanzania. Part I: geology of the Ngozi-Songwe geothermal system. Proc. World Geotherm. Congr. 25–29.

Delvaux D (2001) Karoo rifting in western Tanzania: precursor of Gondwana break-up ? Contrib. to Geol. Palaeontol. Gondwana honour Helmut Wopfner 111–125.

Dypvik H, Nesteby H, Ruden F, Aagaard P, Johansson T, Msindai J, Massay C (1990) Upper Paleozoic and Pesozoic sedimentation in the Rukwa-Tukuyu Region Tanzania. J African Earth Sci 11:437–456. https://doi.org/10.1016/0899-5362(90)90022-7

EAGER, 2018. Enhanced resource modeling at Songwe.

Ebinger CJ (1989) Geological society of America Bulletin Tectonic development of the western branch of the East African rift system. Geol Soc Am Bull 7606:885–903. https://doi.org/10.1130/0016-7606(1989)101%3c0885

Ellis AJ, Wilson SH (1960) The geochemistry of alkali metal ions in the Wairakei hydrothermal system. New Zeal J Geol Geophys 3:593–617. https://doi.org/10.1080/00288306.1960.10420148

Fournier RO (1977) Chemical geothermometers and mixing models for geothermal systems. Geothermics 5:41–50. https://doi.org/10.1016/0375-6505(77)90007-4

Giggenbach WF (1988a) Geothermal solute equilibria. Derivation of Na-K-Mg-Ca geoindicators. Geochim Cosmochim Acta 52:2749–2765. https://doi.org/10.1016/0016-7037(88)90143-3

Giggenbach WF, Soto RC (1992) Isotopic and chemical composition of water and steam discharges from volcanic-magmatic-hydrothermal systems of the Guanacaste Geothermal Province. Costa Rica Appl Geochem 7:309–332. https://doi.org/10.1016/0883-2927(92)90022-U

Giggenbach WF (1988b) Geothermal solute equilibrium, derivation of the Na−K−Mg Geoindicator.pdf. https://doi.org/10.1016/0016-7037(88)90143-3

Harkin D, Harpum J (1978) Geological Map of Tukuyu (QDS 244), in: Tech. Rep. Geological Survey of Tanganyika, Dodoma.

Henley RW, Ellis AJ (1983) Geothermal systems ancient and modern : a geochemical review 19.

Hinz N, Cumming B, Sussman D (2018) Exploration of fault-related deep-circulation geothermal resources in the western branch of the East African Rift System: examples from Uganda and Tanzania. Proc. 7th African Rift Geotherm. Conf. 2018. Kigali, Rwanda. 16 p.

Hochstein MP (1988) Assessment and modelling of geothermal reservoirs (small utilization schemes). Geothermics 17:15–49. https://doi.org/10.1016/0375-6505(88)90004-1

Hochstein M, Temu E, Moshy CM (2000) Geothermal resources of Tanzania. Proc World Geotherm Congr Japan. https://doi.org/10.1016/0375-6505(70)90412-8

James C (1959) Carbon-dioxide-bearing hot springs in the Songwe River Valley, Mbeya District. Tanganyika Geol Surv Rec 7

Kalberkamp U, Schaumann G, Ndonde PB, Chiragwile AS, Mwano MJ, GEOTHERM, working group (2010) Surface Exploration of a Viable Geothermal Resource in Mbeya Area, SW Tanzania. Part III: Geophysics Ulrich. Proc. World Geotherm. Congr.

Kilembe EA, Rosendahl BR (1992) Structure and stratigraphy of the Rukwa rift. Tectonophysics 209:143–158. https://doi.org/10.1016/0040-1951(92)90016-Y

Kraml M, Schaumann G, Kalberkamp U, Stadtler C, Delvaux D, Ndonde P, Mnjokava T, Chiragwile S, Mayalla J, Kabaka K, Mwano J, Makene C (2008) Geothermal Energy as an Alternative Source of Energy for Tanzania, Final Technical Report of Phase I (2006–2009). Technical Cooperation with United Republic of Tanzania

Kraml M, Mnjokava TT, Mayalla WJ, Kabaka K, GEOTHERM G. working (2010) Surface Exploration of a Viable Geothermal Resource in Mbeya Area, SW Tanzania Part II: Geochemistry, In: Proceedings World Geothermal Congress.

Macfarlane A (1966) Geological Map of Itumba (QDS 258), In: Tech. Rep. Mineral Resources Division, Dodoma.

Makundi JS, Kifua GM (1985) Geothermal features of the Mbeya prospect in Tanzania. Geotherm Resour Counc 9:451–454

Minissale A, Donato A, Procesi M, Pizzino L, Giammanco S (2019) Systematic review of geochemical data from thermal springs, gas vents and fumaroles of Southern Italy for geothermal favourability mapping. Earth-Science Rev 188:514–535. https://doi.org/10.1016/j.earscirev.2018.09.008

Mnjokava TT (2007) Interpretation of exploration geochemical data for geothermal fluids from the geothermal field of the rungwe Volcanic Area, SW Tanzania, UNU-GTP Reykjavík, Iceland.

Mtelela C (2018) Preliminary sedimentology and stratigraphy of the enigmatic middle lake beds succession (Pleistocene?) in the Rukwa Rift Basin. Tanzania Tanzania J Sci 44:75–96

Mtelela C, Roberts EM, Downie R, Hendrix MS (2016) Interplay of structural, climatic, and volcanic controls on late quaternary lacustrine-deltaic sedimentation patterns in the Western Branch

of the East African Rift System, Rukwa Rift Basin. Tanzania J Sediment Res 86:1179–1207. https://doi.org/10.2110/jsr.2016.73

Nicholson K (1993) Geothermal fluids: Chemistry and exploration techniques. Springer-Verlag, Berlin Heidelberg. https://doi.org/10.1016/0375-6742(95)90013-6

Nzaro (1970) Geothermics (i97o)-SPECXAL xssu~ 2 U. N. Symposium on the Development and Utilization of Geothermal Resources, Pisa I97o 1039–1043.

Parkhurst DL, Appelo CAJ (2013) Description of Input and Examples for PHREEQC Version 3 — A Computer Program for Speciation, Batch-Reaction, One-Dimensional Transport, and Inverse Geochemical Calculations. U.S. Geological Survey Techniques and Methods, book 6, chapter A43, 497 p. U.S. Geol. Surv. Tech. Methods, B. 6, chapter A43 6–43A

Pisarskii BI, Konev AA, Levi KG, Delvaux D (1998) Alkaline carbon dioxide hydrotherms and strontium-containing travertines in the Songwe River valley (Tanzania). Geol. i Geofiz. 934–941.

Reed M, Nicolas S (1984) Calculation of pH and mineral equilibria in hydrothermal waters with application to geothermometry and studies of boiling and dilution. Geochim Cosmochim Acta 48:1479–1492

Roberts EM, O'Connor PM, Gottfried MD, Stevens N, Kapalima S, Ngasala S (2004) Revised stratigraphy and age of the Red Sandstone Group in the Rukwa Rift Basin. Tanzania Cretac Res 25:749–759. https://doi.org/10.1016/j.cretres.2004.06.007

Roberts EM, O'Connor PM, Stevens NJ, Gottfried MD, Jinnah ZA, Ngasala S, Choh AM, Armstrong RA (2010) Sedimentology and depositional environments of the Red Sandstone Group, Rukwa Rift Basin, southwestern Tanzania: new insight into cretaceous and Paleogene terrestrial ecosystems and tectonics in sub-equatorial Africa. J African Earth Sci 57:179–212. https://doi.org/10.1016/j.jafrearsci.2009.09.002

Semkiwa P, Kalkreuth W, Utting J, Mayagilo F, Mpanju F, Hagemann H (1998) The geology, petrology, palynology and geochemistry of Permian coal basins in Tanzania. 1. Namwele-Mkomolo, Muze and Galula coalfields. Int J Coal Geol 36:63–110. https://doi.org/10.1016/S0166-5162(97)00020-7

SWECO (1978) Reconnaissance of geothermal resources, Report for the Ministry of Water, Energy and Minerals of Tanzania, SWECO, Stockhlom, Sweden and VIRKIR, Reykjavik, Iceland.

Theunissen K, Klerkx J, Melnikov A, Mruma A (1996) Mechanisms of inheritance of rift faulting in the western branch of the East African Rift, Tanzania. Tectonics 15:776–790. https://doi.org/10.1029/95TC03685

Truesdell A, Jones B (1974) WATEQ: A computer program for calculating chemical equilibrium of natural waters. U.S.G.S. J Res 2:233–248

Wilson S (1961) pH of natural hydrothermal solution. Geochim Cosmochim Acta 25:233–235

Wopfner H, Kaaya CZ (1991) Stratigraphy and morphotectonics of Karoo deposits of the northern Selous Basin. Tanzania Geol Mag 128:319–334. https://doi.org/10.1017/S0016756800017593